

## Structure and putative signaling mechanism of Protease activated receptor 2 (PAR2) – A promising target for breast cancer

Kavita Kumari Kakarala<sup>a,\*</sup>, Kaiser Jamil<sup>a</sup>, Vinod Devaraji<sup>b</sup>

<sup>a</sup> Centre for Biotechnology and Bioinformatics (CBB), School of Life Sciences, Jawaharlal Nehru Institute of Advanced Studies (JNIAST), 6th Floor, Buddha Bhawan, M.G. Road, Secunderabad 500003, Andhra Pradesh, India

<sup>b</sup> College of Pharmacy, Madras Medical College, E.V.R. Periyar Salai, Chennai 600003, India



### ARTICLE INFO

#### Article history:

Accepted 21 July 2014

Available online 7 August 2014

#### Keywords:

Homology modeling

Binding affinity

Endogenous ligands

Agonist

Antagonist

### ABSTRACT

Experimental evidences have observed enhanced expression of protease activated receptor 2 (PAR2) in breast cancer consistently. However, it is not yet recognized as an important therapeutic target for breast cancer as the primary molecular mechanisms of its activation are not yet well-defined. Nevertheless, recent reports on the mechanism of GPCR activation and signaling have given new insights to GPCR functioning. In the light of these details, we attempted to understand PAR2 structure & function using molecular modeling techniques. In this work, we generated averaged representative stable models of PAR2, using protease activated receptor 1 (PAR1) as a template and selected conformation based on their binding affinity with PAR2 specific agonist, GB110. Further, the selected model was used for studying the binding affinity of putative ligands. The selected ligands were based on a recent publication on phylogenetic analysis of Class A rhodopsin family of GPCRs. This study reports putative ligands, their interacting residues, binding affinity and molecular dynamics simulation studies on PAR2-ligand complexes. The results reported from this study would be useful for researchers and academicians to investigate PAR2 function as its physiological role is still hypothetical. Further, this information may provide a novel therapeutic scheme to manage breast cancer.

© 2014 Elsevier Inc. All rights reserved.

### 1. Introduction

Increasing incidences of breast cancer are one of the greatest health issues among women. According to the Indian Council of Medical Research (ICMR), the number of cases of breast cancer has nearly doubled in the last 24 years. One in every 22 women is likely to develop breast cancer and increased number of cases are observed among urban women (ICMR Release: <http://www.biospace.com/News/icmr-release-breast-cancer-a-rising-epidemic-in/285374>). India has recorded 70,218 deaths due to breast cancer, which is higher compared to any other nation in the world (Breast Cancer India, <http://www.breastcancerindia.net/>).

Targeted therapy has been successful in treating breast cancer subtypes that express estrogen receptor (ER), progesterone receptor (PR) and human epidermal receptor 2 (HER2). However, it fails in subtypes, which do not express these receptors (ER<sup>-</sup>, PR<sup>-</sup>, and HER2<sup>-</sup>)/triple negative. Although, chemotherapy is employed to

treat triple negative breast cancer, dose-related toxicity and multidrug resistance often result in discontinuation of the treatment. Epidermal growth factor receptor (EGFR), poly(ADP Ribose) polymerase 1 (PARP), insulin like growth factor (IGF1), PI3K/Akt/mTOR signaling pathway, are some of the currently studied therapeutic targets of breast cancer. However, disease-related mortality remains a major concern, mainly because of the heterogeneous nature of breast cancer subtypes and complex mechanisms leading to breast cancer disease. Thus, the recognition of new therapeutic targets is an urgent demand.

Protease activated receptors (PAR2, PAR2, PAR3 & PAR4) belong to the superfamily of G protein coupled receptors (GPCRs) with a unique mechanism of activation, so far not noticed in other GPCRs. PARs play a key role in various physiological and pathophysiological conditions [1].

#### 1.1. PAR2 and breast cancer

PAR2 levels were shown to increase in infiltrative ductal breast cancer tissue and in breast cancer cell line MDA-MB-231 [2]. Up-regulation of PAR2 in proliferating stromal fibroblasts surrounding the carcinoma cells in breast cancers was also reported [3]. PAR2

\* Corresponding author. Tel.: +91 40 27541551; fax: +91 40 27541551.

E-mail addresses: [kavitakakarala@gmail.com](mailto:kavitakakarala@gmail.com), [kavita@jnias.in](mailto:kavita@jnias.in) (K.K. Kakarala).

agonists induced Vascular endothelial growth factor (VEGF) secretion in breast cancer cells [4]. Enhanced PAR2 expression resulted in cellular proliferation, angiogenesis and metastasis in breast cancer and other cancer types [5–11]. Interestingly, Su et al. observed higher PAR2 protein expression in breast tumor specimens and breast cancer cell lines in comparison to normal breast cancer cells/non cancerous breast cancer cell lines. Their work also proved that PAR2 agonist could increase breast cancer cell chemokinesis through the G (alpha)-c-Src-JNK-paxillin signaling pathway [12]. Further, PAR2 was proved to act as an endogenous receptor for factors VIIa and Xa in invasive breast cancer cells and its activation led to increased breast cancer migration [6,13,14]. A recent study has revealed that PAR2 forms protein complexes with β-arresting and other signaling molecules rich in pseudopodia suggesting its role in metastasis of breast cancer cells [15]. Thus, PAR2 represents an attractive therapeutic target for preventing breast cancer.

### 1.2. The challenges in investigating PAR2

Drug development targeting PAR2 has not earned much attention despite many evidences suggesting a key role in the breast cancer disease mechanism. The main reason for this could be attributed to its unique mechanism of activation, mediated by proteases. The proteases known to activate PAR2 are trypsin, tryptase, TF/FVIIa, TF/FVIIa-generated FXa, acrosin, matriptase/MT-SP1, trypsin IV, granzyme A and KLK 2, 4, 5 [16–26]. Activation solely by proteases is a common mechanism which PAR2 shares with other members of the family of protease activated receptors (PAR1, PAR3, PAR4) [17,27]. Protease mediated activation results from the exposure of new N-terminal sequence, termed as Tethered ligand (TL) [28,29]. The interaction of TL with second extracellular loop (ECL<sub>2</sub>) results in a conformational change in the transmembrane domain of the receptor leading to the activation of the receptor [29,30].

Absence of information on the possible endogenous ligands is also responsible for the hypothetical role of PAR2 in physiological as well as pathological conditions. Moreover, identification of potent PAR antagonists has been difficult as these antagonists need to compete with the higher concentration of the tethered agonist generated by proteolytic cleavage [31]. The use of peptide agonist [29,32] and pepducins [33] gave limited insight into PAR2 role, as they get degraded [34]. Nevertheless, recent studies showed comparable agonist activity of the synthetic agonist (GB110) and antagonist (GB88) [34,35] indicating the utility of synthetic ligands in probing PAR2 function, using the structure based drug design methods.

This work describes homology modeling, induced fit docking (IFD), estimation of free energy of ligand binding (Prime/MMGBSA), molecular dynamics simulation study on PAR2 structure and its putative signaling mechanism. The results of this study report for the first time the ligand guided stable three-dimensional structure of PAR2, the binding affinity of putative ligands and important residues that could be targeted further for site directed mutagenesis studies. The detailed analysis of PAR2 structure and its interaction with putative ligands reported in this study would not only be useful in structure based drug design targeting PAR2 against breast cancer but also in interpreting its role in vivo.

## 2. Methodology

**Software:** Molecular modeling was performed using different modules/tools of Schrödinger (Schrödinger, LLC, New York, NY, 2012). Molecular dynamics simulation studies were done using Desmond v. 3.1 (Desmond Molecular Dynamics System, version 3.1,

D.E. Shaw Research, New York, NY, 2012; Maestro-Desmond Interoperability Tools, version 3.1, Schrödinger, New York, NY, 2012).

The flowchart depicts the steps followed in this study (Fig. 1). Detailed description of the steps are available in the following sections.

### 2.1. Homology modeling and validation

PAR2 model was generated using human protease activated receptor (PAR1) (PDBID: 3VW7) (2.2 Å) as a template (44% identity) [31]. Only residues corresponding to the transmembrane domain (Val 76–Asp 350) of PAR2 were modeled using Prime (Prime, version 3.1, Schrödinger, LLC, New York, NY, 2012) [36,37]. The alignment generated by Clustal W [38] was manually edited to remove insertions/deletions in conserved residues of the helices (Fig. 2). The lowest energy model was further refined using loop refinement tool of Prime, followed by minimization using OPLS\_2005 force field [39] (Prime, version 3.1, Schrödinger, LLC, New York, NY, 2012). The homology model of human PAR2 was validated using multiple tools: the Ramachandran plot (Schrödinger, LLC, New York, NY, 2013), PROCHECK [40] available at the PDB sum site (<http://www.ebi.ac.uk/thornton-srv/software/PROCHECK>), ProSA [41,42], ERRAT [43] and Molprobity [44]. This initial model was selected for further molecular dynamics simulation studies, which was followed by studies on the binding affinity of ligands.

### 2.2. Molecular dynamics simulation studies

PAR2 model was pre-equilibrated in the lipid layer composed of POPE (1-palmitoyl-2-oleoyl-Sn-glycero-3-phosphoethanolamine) using the system builder tool of Desmond in Maestro 9.6. The system was set up using the TIP4P explicit solvent model in an orthorhombic simulation box with the 10 Å distance of the buffer in all directions. The system was neutralized, and the ionic strength was set to 0.15 M [45–47].

All the simulations were run in the NPT ensemble, the temperature and pressure was maintained at 300 K and 11.01325 bar respectively by coupling to the Nose-Hoover thermostat and using isotropic coupling [48]. 12 ns and 5 ns simulation time periods were used to study the stability of apoprotein and receptor-ligand complex. Default settings were used for other options (Desmond Molecular Dynamics System, version 3.1, D.E. Shaw Research, New York, NY, 2012; Maestro-Desmond Interoperability Tools, version 3.1, Schrödinger, New York, NY, 2012). The root mean square deviations, and root mean square fluctuations were carried out using a simulation event analysis tool (SEA). SEA panel and the trajectory panel were opened simultaneously for the analysis. Using this option, RMSD of heavy atoms was calculated and later on analyzed with time series option. Similarly, root mean square fluctuations (RMSF) were calculated and analyzed to obtain RMSF plot. The regions corresponding to RMSF were highlighted in the model to observe the residues showing fluctuations (supplementary material, Fig. S3).

### 2.3. Hierarchical clustering

Desmond trajectory clustering (hierarchical clustering) was applied to extract cluster representatives from the trajectory of 10 ns MDS studies. Based on this analysis five representative PAR2 model structures were obtained for further analysis (Desmond Molecular Dynamics System, version 3.1, D.E. Shaw Research, New York, NY, 2012; Maestro-Desmond Interoperability Tools, version 3.1, Schrödinger, New York, NY, 2012).

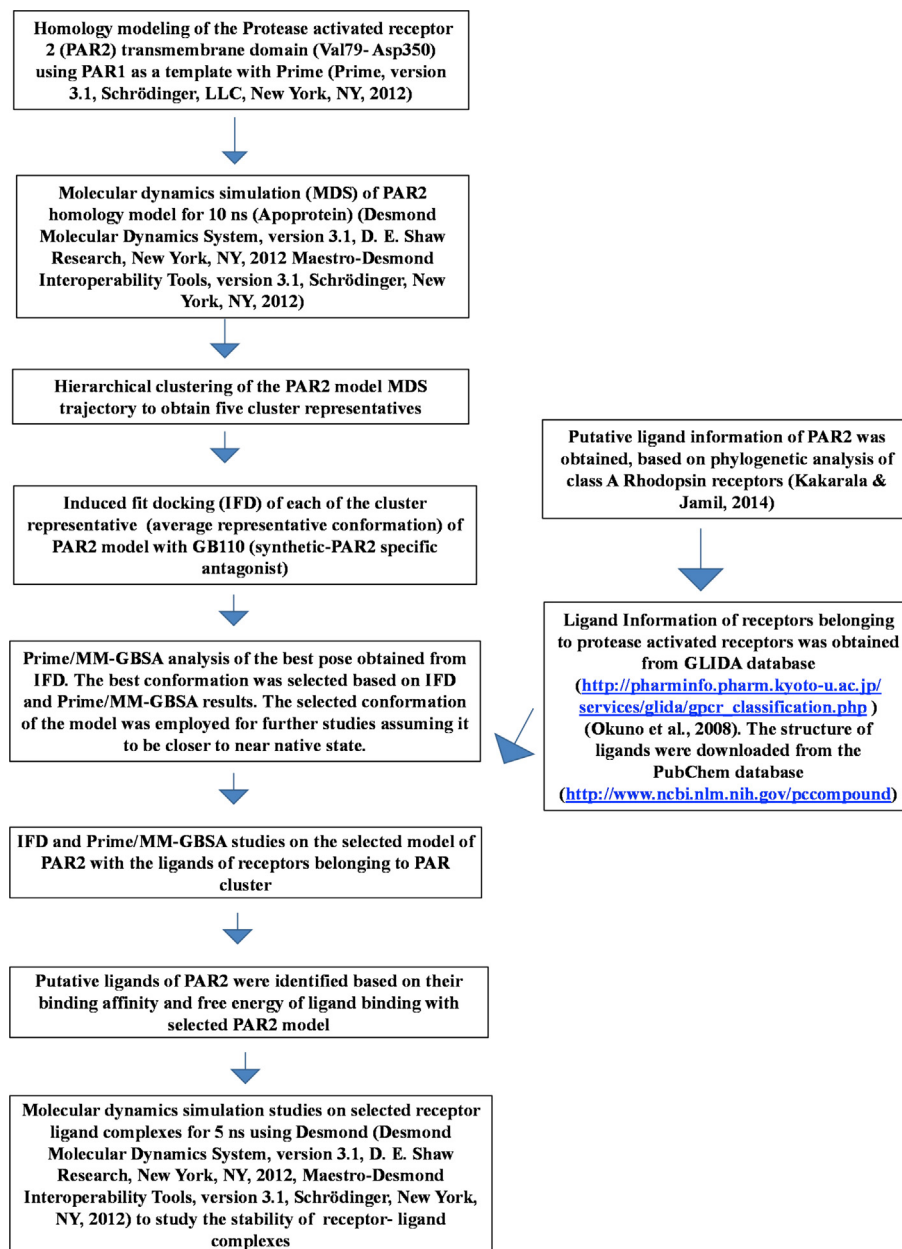


**Fig. 1.** Schematic representation of the workflow.

#### 2.4. Protein preparation

The protein preparation wizard was used to prepare averaged representatives of PAR2 models/selected PAR2 model. The protein preparation wizard prepares the structures by adding missing hydrogen atoms, correcting bond order assignments, charge states and orientation of various groups (Schrödinger Suite 2012 Protein Preparation Wizard; Epik version 2.3, Schrödinger, LLC, New York, NY, 2012; Impact version 5.8, Schrödinger, LLC, New York, NY, 2012; Prime version 3.1, Schrödinger, LLC, New York, NY, 2012).

#### 2.5. Ligand preparation

The potential cognate ligands for protease activated receptors were published recently by our group based on phylogenetic analysis [49]. Based on this study, the information on the ligands of the receptors belonging to PAR2 cluster was obtained from GLIDA database ([http://pharminfo.pharm.kyoto-u.ac.jp/services/glida/gpcr\\_classification.php](http://pharminfo.pharm.kyoto-u.ac.jp/services/glida/gpcr_classification.php)) [50]. The 3D structures of GB110

(PAR2 specific agonist) and the corresponding structures were downloaded from PubChem (<http://www.ncbi.nlm.nih.gov/pccompound>). These structures were prepared with LigPrep tool. Ligand preparation includes a series of steps that perform conversions from 2D to 3D, apply corrections to the structure, produce ionization states at biological pH, generate possible tautomers, optimize the geometries and finally minimize the ring conformations (LigPrep, version 2.5, Schrödinger, LLC, New York, NY, 2012).

#### 2.6. Induced fit docking

Induced fit docking (IFD), which combines Glide and the Refinement module in Prime, was used for the docking studies. Receptor grid was generated around following residues; Tyr 310<sup>6,59</sup>, Tyr 344<sup>7,53</sup>, Phe 244<sup>5,39</sup>, His 228 (ECL<sub>2</sub>) and Asp 229 (ECL<sub>2</sub>). These residues are the corresponding binding site residues identified in PAR1 (template) [31]. 20 poses per ligand were generated in the initial Glide docking step using stranded precision (SP) method, with

Residues not modeled		
sp P25116 PAR1_HUMAN	MGPRRLLLVAACFSLCGPLLSARTRARRPESKATNATLDPRSFLLRNPNDKYEPFWEDEE	60
sp P55085 PAR2_HUMAN	-----MRSPSAWLLGAAILLAASLSCSGTIQGTONRSSKGRSLIGKVDG-----TSH	47
Residues not modeled		
sp P25116 PAR1_HUMAN	KNESGLTEYRLVSINKSSPLQKQLPAFISEDASGYLTSSWLTLFVPSVYTGTVFVVSLPLN	120
sp P55085 PAR2_HUMAN	VTGKGTVETVF SVDEFS-----ASVLTGKLTTVFLPIVYTIVFVVGLPSN	93
ICL1 TM2 ECL1		
sp P25116 PAR1_HUMAN	IMAIIVVFI <span style="color: red;">LK</span> MKVKKPA <span style="color: green;">VVYMLH</span> LATADVL <span style="color: red;">FV</span> S <span style="color: green;">VLPF</span> K <span style="color: red;">ISYYF</span> SGSDWQFG <span style="color: green;">SELCRFVTA</span>	180
sp P55085 PAR2_HUMAN	GMALWVF <span style="color: red;">LF</span> R <span style="color: blue;">TKKKHPA</span> VIYMAN <span style="color: red;">LALAD</span> LLS <span style="color: green;">VIWFPLKIA</span> YHI <span style="color: red;">HGNNWIYGEALCNVLIG</span>	153
TM3 ICL2 TM4		
sp P25116 PAR1_HUMAN	AFYC <span style="color: red;">CNMYASILLMTVISIDRF</span> LA <span style="color: red;">V</span> YPM-----RT <span style="color: red;">LGRASF</span> T <span style="color: green;">CLAIWALAIAGV</span> V <span style="color: red;">PLL</span> LKE	240
sp P55085 PAR2_HUMAN	FFY <span style="color: red;">GNMYSILF</span> MT <span style="color: blue;">CLSV</span> QRY <span style="color: red;">WVIVNPMGHSRKKA</span> NIAIGISLAI <span style="color: red;">WLLI</span> LLVTIPLYVVK	212
ECL2 TM5		
sp P25116 PAR1_HUMAN	QT <span style="color: red;">IQV</span> PG <span style="color: green;">LNITTC</span> HD <span style="color: blue;">DVLNET</span> LI <span style="color: red;">GYYAYY</span> FA <span style="color: red;">SAF</span> AVFFF <span style="color: red;">VPLI</span> I <span style="color: green;">ST</span> VC <span style="color: red;">YVSI</span> I <span style="color: red;">RCL</span> SSA	300
sp P55085 PAR2_HUMAN	QT <span style="color: red;">IFIPALN</span> IT <span style="color: blue;">TC</span> HD <span style="color: red;">DVLPE</span> Q <span style="color: green;">ILLVGDMF</span> NY <span style="color: red;">FLSLAIGV</span> F <span style="color: red;">LFP</span> A <span style="color: green;">FT</span> AS <span style="color: red;">AYV</span> LM <span style="color: red;">IRMLRSSA</span>	272
ICL3 TM6 ECL3		
sp P25116 PAR1_HUMAN	---AN <span style="color: red;">RSKKSR</span> AL <span style="color: red;">FLSAA</span> VF <span style="color: red;">CIFI</span> I <span style="color: red;">CFGPT</span> T <span style="color: red;">NVLLIAHYS</span> FL <span style="color: red;">SHT</span> ST <span style="color: red;">TE</span> E <span style="color: red;">AAYFAY</span> LL <span style="color: red;">CV</span> C	358
sp P55085 PAR2_HUMAN	MDENS <span style="color: red;">EKKRKRAIKL</span> IV <span style="color: red;">TVI</span> AMY <span style="color: red;">LIC</span> FT <span style="color: red;">PSN</span> LLL <span style="color: red;">VVHY</span> -FL <span style="color: red;">I</span> K <span style="color: red;">SQG</span> SH <span style="color: red;">VY</span> AL <span style="color: red;">YI</span> VAL <span style="color: red;">CL</span>	331
TM7 Residues not modeled		
sp P25116 PAR1_HUMAN	SS <span style="color: red;">ISCC</span> IDI <span style="color: red;">PLI</span> YYY <span style="color: green;">ASSE</span> C <span style="color: red;">QRYV</span> Y <span style="color: green;">SIL</span> CC <span style="color: red;">KESS</span> DP <span style="color: green;">SSY</span> NS <span style="color: red;">SQL</span> MA <span style="color: red;">SKMD</span> T <span style="color: green;">CSS</span> N <span style="color: red;">LNNSI</span>	418
sp P55085 PAR2_HUMAN	STLN <span style="color: red;">SCIDP</span> F <span style="color: red;">VYY</span> F <span style="color: green;">SHD</span> FRDHAK <span style="color: red;">NALL</span> CR <span style="color: red;">S</span> V <span style="color: green;">RTV</span> K <span style="color: red;">QM</span> Q <span style="color: green;">S</span> L <span style="color: red;">TSK</span> H <span style="color: red;">SR</span> K <span style="color: green;">SSY</span> SS <span style="color: red;">SS</span> STT	391
sp P25116 PAR1_HUMAN	YKKLLT 425	
sp P55085 PAR2_HUMAN	V <span style="color: green;">KTSY</span> - 397	

**Fig. 2.** Multiple sequence alignment of PAR2 with PAR1 (template). The alignment generated by Clustal W and GPCR specific alignment in Prime 3.1 was finally edited to remove insertions and deletions in the helices. The residues corresponding to transmembrane helices are shown in red and that of the loop region in black. Residues in  $\beta$  strands are represented in blue, and the residues that were not modeled are represented in green. QSLSW represents residues with missing coordinates in PAR1 (template). (For interpretation of the references to color in this figure legend, the reader is referred to the web version of this article.)

the van der Waals (vdW) radii scaled to 0.5. In the next stage, for each docking pose, protein refinement was performed with Prime 3.1 on residues in the range of 5 Å in all the 20 poses. Based on the energy calculated by Prime, the obtained complexes were ranked and those poses with less than 30 kcal/mol energy were selected for the redocking step with Glide XP.

Selection of the best poses depended on the Glide score [Glide score (G-score) in kcal/mol, which is calculated as follows: G-Score = H bond + Lipo + Metal + Site + 0.130 Coul + 0.065vdW – Bury P – RotB, where Hbond = Hydrogen bonds, Lipo = Hydrophobic interactions, Metal = Metal binding term, Site = Polar interactions in the binding site, vdW = van der Waals forces, Coul = coulombic forces, Bury P = Penalty for the buried polar group, RotB = Freezing rotatable bonds] and the relative energy of interaction calculated by IFD score (IFD score = GlideScore + 0.05 × Prime eEnergy) (Schrödinger Suite 2012 Induced Fit Docking protocol; Glide version 5.8, Schrödinger, LLC, New York, NY, 2012; Prime version 3.1, Schrödinger, LLC, New York, NY, 2012). The best pose was also selected on the basis of the position and conformation of the ligand within the binding pocket, key hydrogen bonding and  $\pi$ – $\pi$  stacking interactions.

### 2.7. Prime/MM-GBSA binding-free energy computation

The best poses selected were further analyzed by Prime/MM-GBSA method to calculate the free energy of ligand binding in the receptor-ligand complex [51].

The total free energy of binding is calculated as follows:  $\Delta G_{\text{bind}} = G_{\text{complex}} - (G_{\text{protein}} + G_{\text{ligand}})$ , where  $G = \text{MME}$  (molecular mechanics energies) + GSGB (SGB solvation model for polar solvation) + GNP (nonpolar solvation) (Prime, version 3.1, Schrödinger, LLC, New York, NY, 2012).

### 2.8. Number system of amino acids

The numbers above the single letter code of amino acids indicate the Ballesteros Weinstein numbering [52] and the one below corresponds to the number assigned by Schrödinger software (Fig. 3).

## 3. Results and discussion

PAR2 has a regulatory role in several signaling pathways mediated by c-Jun N-terminal kinase (JNK), toll-like receptor 3, tumor necrosis factor, extracellular-signal-regulated kinases 1&2 (ERK1 and ERK2), I-kappaB kinase/NF-kappaB, phosphatidylinositol 3-kinase, toll-like receptor 4, etc. (<http://www.uniprot.org/uniprot/P55085>) [53]. Further, PAR2 activation was reported to result in up/down-regulation of 1000 genes that are important in cell metabolism, the cell cycle, the MAPK pathway, HDAC and sirtuin enzymes, inflammatory cytokines, and anti-complement function along with upregulation of genes important in cancer [54]. Interestingly, most of these signaling pathways are targets in breast cancer therapy. Thus, data on PAR2 structure and mechanism of activation could greatly

>sp P55085 PAR2_HUMAN_76-350																																
1.33	1.34	1.35	1.36	1.37	1.38	1.39	1.40	1.41	1.42	1.43	1.44	1.45	1.46	1.47	1.48	1.49	1.50	1.51	1.52	1.53	1.54	1.55	1.56	1.57	1.58							
V	F	L	P	I	V	Y	T	I	V	F	V	G	L	P	S	N	G	M	A	L	W	V	F	L								
76	77	78	79	80	81	82	83	84	85	86	87	88	89	90	91	92	93	94	95	96	97	98	99	100	101							
1.59																																
F	R	T	K	K	K	H	P	A	V	I	Y	M	A	N	L	A	L	A	D	L	L	S	V	I	W							
102	103	104	105	106	107	108	109	110	111	112	113	114	115	116	117	118	119	120	121	122	123	124	125	126	127							
2.57	2.58	2.59	2.6	2.61	2.62	2.63	2.64	2.65	2.66	2.67							3.22	3.23	3.24	3.25	3.26	3.27	3.28	3.29	3.30							
F	P	L	K	I	A	Y	H	I	H	G	N	N	W	I	Y	G	E	A	L	C	N	V	L	I	G							
128	129	130	131	132	133	134	135	136	137	138	139	140	141	142	143	144	145	146	147	148	149	150	151	152	153							
3.31	3.32	3.33	3.34	3.35	3.36	3.37	3.38	3.39	3.40	3.41	3.42	3.43	3.44	3.45	3.46	3.47	3.48	3.49	3.50	3.51	3.52	3.53	3.54									
F	F	Y	G	N	M	Y	C	S	I	L	F	M	T	C	L	S	V	Q	R	Y	W	V	I	V	N							
154	155	156	157	158	159	160	161	162	163	164	165	166	167	168	169	170	171	172	173	174	175	176	177	178	179							
P	M	G	H	S	R	K	K	A	N	I	A	I	G	I	S	L	A	I	W	L	L	I	L	L	V							
180	181	182	183	184	<u>185</u>	<u>187</u>	188	189	190	191	192	193	194	195	196	197	198	199	200	201	202	203	204	205	206							
4.57	4.58	4.59	4.60	4.61																												
T	I	P	L	Y	V	V	K	Q	T	I	F	I	P	A	L	N	I	T	T	C	H	D	V	L	P							
207	208	209	210	211	212	213	214	215	216	217	218	219	220	221	222	223	224	225	226	227	228	229	230	231	232							
E	Q	L	L	V	G	D	M	F	N	Y	F	L	S	L	A	I	G	V	F	L	F	P	A	F	L							
233	234	235	236	237	238	239	240	241	242	243	244	245	246	247	248	249	250	251	252	253	254	255	256	257	258							
5.54	5.55	5.56	5.57	5.58	5.59	5.60	5.61																									
T	A	S	A	Y	V	L	M	I	R	M	L	R	S	S	A	M	D	D	D	S	E	K	K	R	K							
259	260	261	262	263	264	265	266	267	268	269	270	271	272	273	274	275	276A	276B	276C	277	278	279	280	281	282							
6.32	6.33	6.34	6.35	6.36	6.37	6.38	6.39	6.40	6.41	6.42	6.43	6.44	6.45	6.46	6.47	6.48	6.49	6.50	6.51	6.52	6.53	6.54	6.55	6.56	6.57							
R	A	I	K	L	I	V	T	V	L	A	M	Y	L	I	C	F	T	P	S	N	L	L	V	V	V							
283	284	285	286	287	288	289	290	291	292	293	294	295	296	297	298	299	300	301	302	303	304	305	306	307	308							
6.58	6.59																7.29	7.30	7.31	7.32	7.33	7.34	7.35	7.36	7.37	7.38	7.39	7.40	7.41	7.42	7.43	7.44
H	Y	F	L	I	K	S	Q	G	Q	S	H	V	Y	A	L	Y	I	V	A	L	C	L	S	T	L							
309	310	311	312	<u>313</u>	<u>315</u>	316	317	318	319	320	321	322	323	324	325	326	327	328	329	330	331	332	333	334	335							
7.45	7.46	7.47	7.48	7.49	7.50	7.51	7.52	7.53	7.54																							
N	S	C	I	D	P	F	V	Y	Y	F	V	S	H	D																		
336	337	338	339	340	341	342	343	344	345	346	347	348	349	350																		

**Fig. 3.** Numbering of amino acid residues in PAR2 sequence. Ballesteros Weinstein numbering of the residue is mentioned above the single letter code of amino acid. The number given below the single letter code of amino acid is based on PAR2 sequence information in Uniprot database (<http://www.uniprot.org/uniprot/P55085>). Underlined residues show the positions where discontinuous numbers were assigned by Schrödinger software.

increase our understanding of this unique receptor, playing a key function in breast cancer.

Homology models were successful in predicting the correct three-dimensional structure of GPCRs and receptor ligand information, e.g.  $\beta$ 2 adrenergic receptor, adenosine A2A receptor, dopamine, etc. [55–57]. The recent review on GPCR structure based drug design elegantly described many aspects from structure prediction to structure based drug design. Further, the authors described molecular modeling as a tool to understand GPCR structure and function [58]. PAR2 crystal structure is not available yet, and the reported homology model of PAR2 was based on the crystal structure of rhodopsin [59]. Although rhodopsin belongs to the superfamily of GPCRs, it may not be the appropriate template to model PAR2, as it does not share the unique mechanism of activation. Thus, the PAR2 model generated from closely related template PAR1 would be closer to the physiological structure as it belongs to the same subfamily with similar activation scheme. Therefore, we suggest that the PAR2 model generated in our study may be most appropriate for structure based drug design methods.

### 3.1. PAR2 homology modeling and validation

GPCR modeling based on multiple templates was not useful in structure prediction when closely related single template is available [60,61]. Therefore, the homology model of PAR2 based on PAR1 was generated using Prime 3.1 (refer Section 2.1). PAR2 homology model showed the typical structure of GPCRs, i.e. seven transmembrane helices with three extracellular (ECLs) and

intracellular loops (ICLs). Of the three extracellular loops (ECLs), the second extracellular loop (ECL<sub>2</sub>) showed two anti-parallel  $\beta$  strands with hairpin conformation projecting away from the binding cavity. PAR1, chemokine (CXCR4) and opioid receptors also showed two anti-parallel  $\beta$  strands in ECL<sub>2</sub> [31,62–64]. In GPCRs, the structural differences between known structures are large in ECL<sub>2</sub> region, which is one of the binding sites [65], hence accurate modeling of ECL<sub>2</sub> is important. The loop prediction/refinement program of Prime works on a robust Protein Local Optimization Program (PLOP). PLOP accurately predicted loops from 4 to 12 residues in GPCRs [33,66,67]. Interestingly, ECL<sub>2</sub> in PAR2 lacked insertions/deletions, minimizing inaccuracies in the loop modeling (Fig. 2). Moreover, the deletions in the ICL<sub>2</sub> and ICL<sub>3</sub> were built based on the PLOP algorithm in the Prime refinement module. After the loop refinement and minimization, structure was validated using protein validation tools (refer Section 2.1).

Ramachandran plot (Schrödinger, LLC, New York, NY, 2013) and PROCHECK validation showed that in PAR2 model, most of the residues were in the allowed region, and the other stereochemical parameters are within the accepted limits, corresponding to native protein structures (Fig. 4) and (supplementary material, S1–S10). Interestingly, for most proteins, Ramachandran plot validation is useful in evaluating the quality of the protein structure predicted but, there are cases where there are violations. In such cases, there might be additional interactions, which stabilize the protein structure [68]. The results of ProSA (score = -3.9) [41,42] and ERRAT (Score = -88.9%) [43] (supplementary material, Figs. S1 and S2) reconfirmed the accuracy of the modeled structure. Molprobity

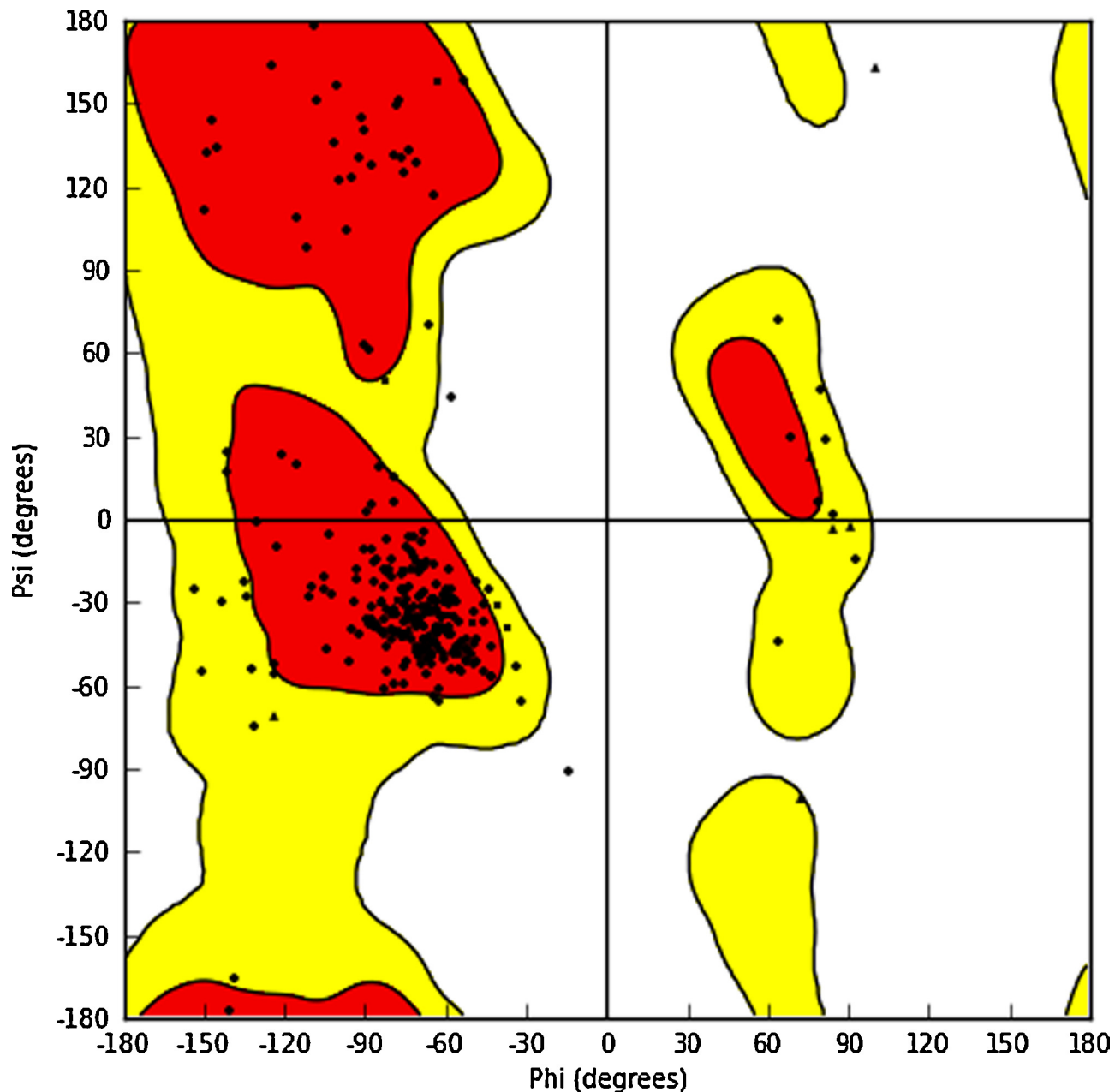


**Fig. 4.** Ramachandran map of PAR2 model. Ramachandran plot was used to validate PAR2 model. The red region shows the allowed regions and yellow area depicts the additionally allowed regions. Most of the residues in PAR2 model were in the allowed region, thus proving that stereochemical parameters are in the acceptable limits in PAR2 model. (For interpretation of the references to color in this figure legend, the reader is referred to the web version of this article.)

evaluation of PAR2 models indicated that 98.9% of the residues fall in the allowed regions of Ramachandran plot and three residues Thr 104, Met 181 and Ser 316 were outliers (supplementary material, S11). Among these residues, Thr 104 is located in the ICL<sub>1</sub> region, Met 181 in ECL<sub>1</sub> region and Ser 316 in the ECL<sub>3</sub> region respectively. Thr 104 residue in PAR2 was aligned with Met 131 of PAR1 and interestingly, this residue was an outlier in the crystal structure of PAR1. Further, Met 181 of PAR2 is in the ICL<sub>2</sub> region where the electron density in the crystal structure was itself not clear [31]. The other residue, Ser 316 is in the ECL3 loop region and interestingly, serine happens to be one the residues associated with the highest propensity to be in the disallowed regions of the Ramachandran plot [68]. As the results from different validation methods were within the acceptable range, PAR2 model (initial model) was selected for further analysis.

### 3.2. Molecular dynamics simulation (MDS) of PAR2 model (APO protein)

Molecular dynamics simulations (MDS) are useful in the analysis of protein ligand interactions in homology models as well as in X-ray crystal structures [69]. MD simulations, both classical at long time scales and simulations involving biasing techniques or reduced representations, are helpful to rationalize biophysical phenomena of membrane proteins in general and GPCRs in particular, giving valuable insights into the GPCR function [70]. In this study, the initial model of PAR2, obtained from Prime 3.1, was subjected to MDS for 10 ns using Desmond (refer Section 2.2). The system setup, software and the parameters employed in the MDS of PAR2 model have been used earlier to elucidate the structural details of S1P3 receptor homology model [71]. Molecular dynamics

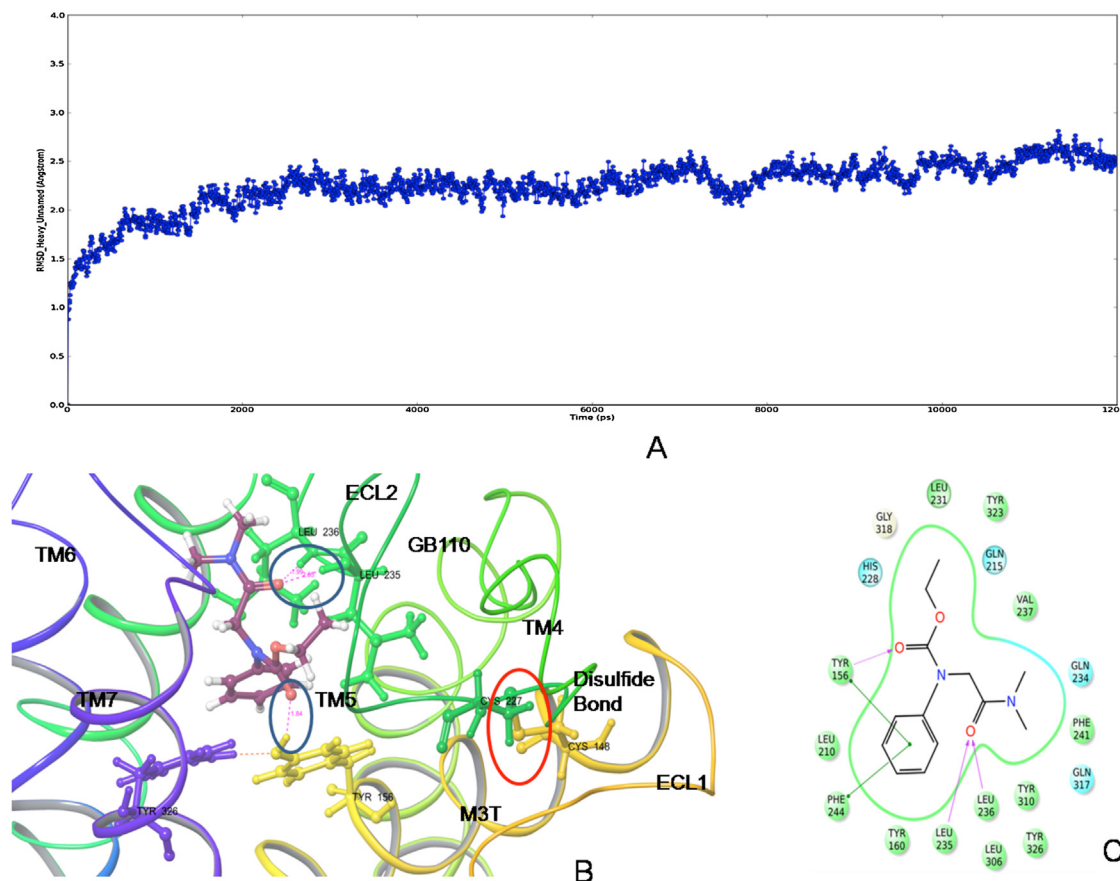


**Fig. 5.** (A) Heavy atom root mean square deviation (RMSD) plot was generated for the 12 ns MDS trajectory of PAR2 model. RMSD plot of heavy atoms of the PAR2 model with time shown in ps along X-axis and RMSD values in Å along Y-axis is shown. Molecular dynamics (MD) simulation was run using Desmond v 2.4 (refer Section 2.2). (B) Binding pose of PAR2-GB110 (PAR2 specific agonist) complex. Hydrogen bonding interactions between GB110 and residues of PAR2 model (Leu 235 (ECL<sub>2</sub>), Leu 236 (ECL<sub>2</sub>) and Tyr 156<sup>3.33</sup>) are shown as pink dashed lines and is highlighted in blue circles. The disulfide bond between Cys 148<sup>3.25</sup> and Cys 227 (ECL<sub>2</sub>) is depicted in red circle. (C) LigPlot diagram of PAR2-GB110 interaction. Hydrogen bonding interactions between GB110 and Leu 235 (ECL<sub>2</sub>), Leu 236 (ECL<sub>2</sub>) and Tyr 156<sup>3.33</sup> is shown. The hydrogen bond interactions are shown as pink arrows and the π-π interaction with Tyr 156<sup>3.33</sup> and Phe 244<sup>5.39</sup> of PAR2 model are depicted by green lines. (For interpretation of the references to color in this figure legend, the reader is referred to the web version of this article.)

simulation was carried out for 12 ns, however the time period of 10 ns was selected to study PAR2 model stability as Raval et al. [72] had noted that the homology models, drift away from the native structure under long molecular dynamics simulations and hence limiting sampling close to the initial model, could lead to improvement [72]. The final RMSD variation from the initial model of heavy atoms show that system is stable beyond 10 ns (Fig. 5A). For hierarchical clustering, we have considered MDS trajectory for 10 ns. Moreover, we observed that within 10 ns the model had reached stable local minima by 4 ns in the MDS of PAR2 model. Further, it was observed that 3 ns molecular dynamics simulation was enough to reach one stable local minima and the structure corresponding to this time period was able to discriminate binding affinity of homology models of dopamine D2 and dopamine D3 [73].

Root mean square fluctuations (RMSF) were largely limited to loops. These flexible regions corresponded in to ICL<sub>1</sub> (Leu 101–His 108), ECL<sub>1</sub> (His 137–Gly 144), ICL<sub>2</sub> (Val 176–Lys 188), ECL<sub>2</sub> ((Leu 214), (Phe 218–Tyr 224), (Gln 234), (Val 237), (Phe 254), (Phe 257), residues close to ICL<sub>3</sub> (Leu 265), ICL<sub>3</sub> (Arg 268–Lys 282) and residues at the interface of TM6/TM7 and ECL<sub>3</sub> (Phe 311–Val 322) respectively (supplementary material, Fig. S3).

### 3.3. Clustering of conformers – prediction of near native conformation of PAR2 model

Earlier investigations have shown the utility of incorporating ligand based information in successful prediction of native

contacts; in this method, known ligands were docked to the initial model. Then, multiple conformations of receptor-ligand complexes were clustered based on energy, and the lowest energy model was selected for further study [74,75]. Ligand steered homology models were shown to reproduce the experimental binding modes and perform well in the docking analysis, on par with crystal structures [76,77]. This methodology was successful in identifying agonist and antagonist of cannabinoid receptor [78,79]. Selection of near native protein-ligand conformation using hierarchical clustering by analyzing only a reduced set of representative solutions was proved useful in picking up the right pose [80]. In this work, hierarchical clustering method was employed to generate five representative structures from multiple conformations obtained from the MDS of PAR2 receptor model. In the following step, each of the five representative structures of the initial model were docked with experimentally proven PAR2 specific agonist GB110 using IFD (refer Section 2.6). GB110 was chosen because it is the only experimentally proven non-peptidic PAR2 specific agonist and is equipotent in vitro in comparison with the synthetic peptide agonist [33,34].

The IFD docking generated different poses of the PAR2 representative models-GB110 complex. The various poses were ranked based on IFD score (refer Section 2.6). The best docked pose for each representative structure was selected based on visual inspection and the scores generated by Glide and IFD. Glide score is an empirical scoring function that includes force field (electrostatic, van der Waals) contributions in addition to terms like hydrogen bond, hydrophobic interactions and other interactions that

**Table 1**

Binding affinity studies of GB110 with cluster representatives of PAR2 obtained from hierarchical clustering of MDS trajectory for 10 ns. The Glide score and the Prime/MMGBSA dG bind values are given. PAR2 model corresponding to cluster representative 2 was selected for further analysis.

Trajectory cluster representatives	Glide score	Prime/MMGBSA dG Bind (kcal/mol)
Cluster 1	-7.7	-82.5
Cluster 2	-9.7	-92.2
Cluster 3	-8.4	-86.7
Cluster 4	-8.7	-83.1
Cluster 5	-8.0	-64.3

influence ligand binding (refer Section 2.6). Glide is standardized for docking accuracy, database enrichment, and binding affinity prediction [81]. Glide was shown to be more accurate in predicting binding mode of ligands in comparison to GOLD, FlexX and Surflex method [81]. Further, flexible docking program, IFD [82] is known to predict active site geometries with accuracy in crystal structures [83,84] and in homology models of GPCRs and other proteins [85–87].

The best pose thus selected was evaluated for free energy of ligand binding using Prime/MM-GBSA method (refer Section 2.7). This process was chosen as molecular docking combined with Prime/MM-GBSA results was reported to provide ranking comparable to experimental binding affinity [88,89]. Finally, based on the analysis of IFD results and free energy of ligand binding, the binding pose of the PAR2 homology model corresponding to cluster representative 2-GB110 complex, was selected for further docking analysis (Table 1).

Analysis of the binding pose corresponding to selected cluster 2 representative PAR2-GB110 complex obtained from IFD, showed stable hydrogen bonding interaction with Leu 235 (ECL<sub>2</sub>) and Leu 236 (ECL<sub>2</sub>) and Tyr 156<sup>3,33</sup> (Fig. 5B and C). The complex was also stabilized by π–π interaction with Tyr 156<sup>3,33</sup> and Phe 244<sup>5,39</sup>. Interestingly, these residues were reported to exert weak hydrophobic interactions with Vorapaxar in PAR1 [31], suggesting that the predicted PAR2 homology model may be correct.

Thus, the homology model predicted from our study derived from the MDS, hierarchical clustering, binding conformation of experimentally proved agonist GB110 and free energy of ligand binding has a higher probability of having structure close to a stable near native conformation. The docking confirmation of PAR2 model corresponding to selected pose of cluster 2 representatives-GB110 complex was selected for further analysis and is referred as PAR2 model in the following sections of the study.

#### 3.4. PAR2 structure-stabilizing interactions

Analysis of the PAR2 homology model showed that there were several inter-helical hydrogen bonds that may give stability to the structure (Fig. 6A). Intra-molecular disulfide bonds occur within a polypeptide chain and are usually responsible for stabilizing tertiary structures of proteins. In the homology model of PAR2 Cys 148<sup>3,25</sup> of TM3 and Cys 227 of ECL<sub>2</sub> formed a conserved disulfide bond (Fig. 5B). The presence of conserved disulfide bonds in our model suggests that the model may be correct.

The inter-helical hydrogen bonding interactions observed in PAR2 model that may be important in giving structural stability, ligand binding and in signaling are as follows (the numbers within brackets indicate hydrogen bonding distance): Hydrogen bonding interaction between His 135<sup>2,64</sup> and Asn 139 (ECL<sub>1</sub>) (2.12 Å) may stabilize ECL<sub>1</sub> in its position. Glu 145<sup>3,22</sup> present on the top of TM3 is bonded with Lys 214 (ECL<sub>2</sub>) (1.81 Å) and Thr 216 (ECL<sub>2</sub>) (1.74 Å) present on the first strand in the anti parallel β sheet forming ECL<sub>2</sub>. Interestingly, the hydrogen bonding interaction was

observed between Lys 214 (ECL<sub>2</sub>), Gln 215 (ECL<sub>2</sub>) and His 228 (ECL<sub>2</sub>) (1.75 Å). Thus, these residues could be very crucial in holding ECL<sub>2</sub> in its conformation and may facilitate binding of TL to ECL<sub>2</sub>, which is an important event in the PAR2 activation (Fig. 6A and B). The hydrogen bonding interaction between Thr 207<sup>4,57</sup>–Tyr 211<sup>4,61</sup> (2.075 Å), Ser 320<sup>7,29</sup>–Gln 319 (ECL<sub>2</sub>) (1.243 Å), Tyr 156<sup>3,33</sup>–Tyr 326<sup>7,35</sup> (1.809 Å), Tyr 160<sup>3,37</sup> and Asn 303<sup>6,52</sup> (1.935 Å) appears to be important in giving stability to the PAR2 inactive state (Fig. 6C and D). Extensive hydrogen bonding was observed between various residues which included residues of tyrosine switch (described in Section 3.6). The residues and their interacting partners are as follows: Tyr 344<sup>7,53</sup>–Asn 93<sup>1,50</sup> (1.82 Å), Asn 93<sup>1,50</sup>–Asp 121<sup>2,50</sup> (1.867 Å)–Asp 340<sup>7,49</sup> (1.719 Å). Asp 121<sup>2,50</sup> is in turn connected with Asn 336<sup>7,45</sup> (1.668 Å) and Ser 337<sup>7,46</sup> (1.859 Å) while the other end is connected to Asn 158<sup>3,35</sup> (2.235 Å); thus Asp 121<sup>2,50</sup> forms a bridge between TM3 and TM1 and TM7 (Fig. 6C and D). This hydrogen bonding network, involving the residue Asp<sup>7,49</sup> forming a part of the Tyrosine switch, was also observed in the PAR1 crystal structure. Thus, this is one more evidence that the PAR2 homology model could be correct. The other interaction involved is Glu 278<sup>6,27</sup>–Lys 282<sup>6,31</sup> (1.590 Å) and Arg 281<sup>6,30</sup> (1.626 Å). The base of ICL<sub>3</sub> is stabilized by the interaction between Ser 277 (ICL<sub>3</sub>) and Asp 276 (ICL<sub>3</sub>) (2.27 Å) (Fig. 6E and F). Thus, as most of the hydrogen bonding interactions involving conserved residues were observed in the homology model of PAR2, we suggest that the predicted structure of PAR2 may be correct.

#### 3.5. The molecular switches in PAR2

Current understanding of GPCR activation mechanism gives clear evidence that the whole process is more than the role-played by the molecular switches [90–92]. Nevertheless, some information could be obtained by examining the residues of molecular switches and their bonding interactions.

##### 3.5.1. The ionic lock switch (D/QR<sup>3,50</sup> Y motif)

The stabilizing effects of strong electrostatic interactions, centered on the residues in the E/DRY motif, are known in high resolution structures, e.g. inactive rhodopsin structure, dopamine D3 receptor, adenosine A<sub>2A</sub> receptor. However, it is absent in many GPCRs, e.g. in human β2-adrenergic receptor (β2-AR), turkey β1-adrenergic receptor (β1-AR), histamine H1 receptor, etc. as reviewed in [93]. In PAR1, D<sup>3,49</sup> RY (199–201) motif is not stabilized by any hydrogen bonding interaction, whereas, in PAR2, D<sup>3,49</sup> RY is replaced by QR<sup>3,50</sup> Y (172–174) and Gln 172<sup>3,49</sup> is connected to His 183 (ICL<sub>2</sub>). Interestingly, Tyr 174<sup>3,51</sup> showed a different conformation (facing upwards, toward the extracellular part) in comparison to PAR1. Therefore, we suggest that the hydrogen bond between residues Gln 172<sup>3,49</sup> and His 183 (ICL<sub>2</sub>) may stabilize the ionic lock by restraining a helical conformation of ICL<sub>2</sub>. Thus, the residue differences clubbed with difference in the bonding pattern observed in PAR2 suggest that it may have different mechanisms of activation. Further, due to the presence of additional bonds, its activity might also be tightly regulated (Fig. 7).

##### 3.5.2. The 3-7 lock switch (Y<sup>3,33</sup>–Y<sup>7,35</sup> motif)

The 3-7 switch is broken during activation, hence plays an important functional role. In PAR2, the hydrogen bond interaction between Tyr 156<sup>3,33</sup> with Tyr 326<sup>7,35</sup> may act as 3-7 lock switch. Although the opening of ionic lock is important for activation, there seem to be many more variations in the function associated with the operation of this lock.

##### 3.5.3. Transmission switch (Y<sup>6,44</sup>xxCF<sup>6,48</sup>xP<sup>6,50</sup> motif)

Transmission switch plays an important role in activation of GPCRs. It was predicted to act as a toggle switch during

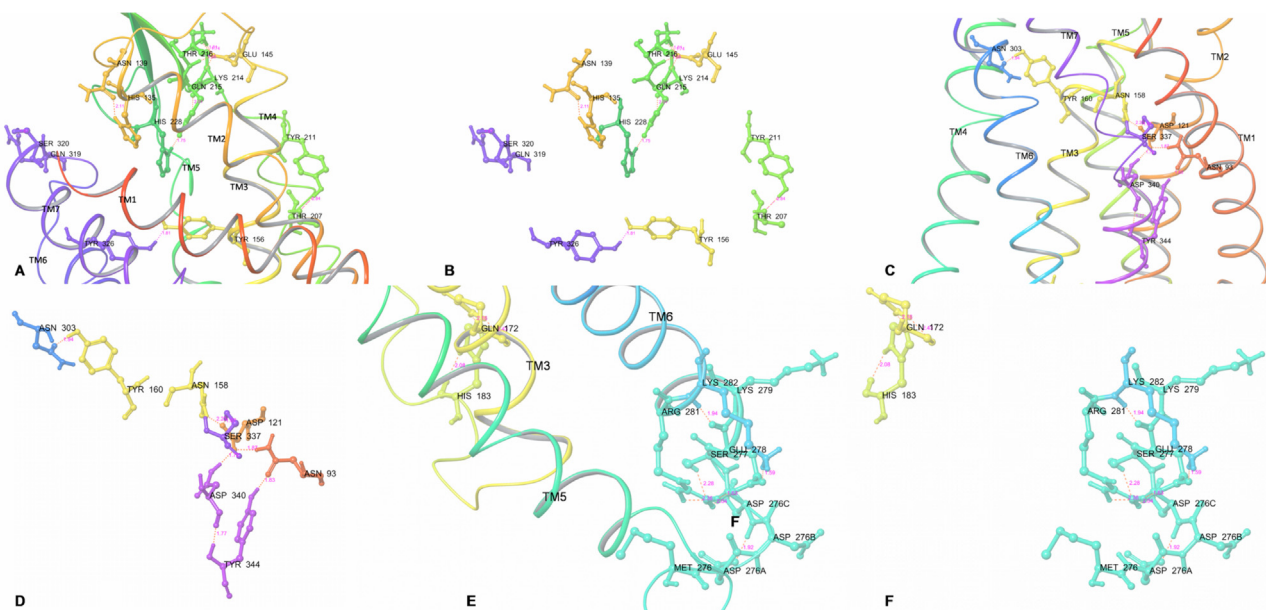


**Fig. 6.** Hydrogen bonding interactions observed in PAR2 model that may stabilize PAR2 structure are shown. (A and B) The hydrogen bonding interactions that are predicted to stabilize the extracellular facing part of the PAR2 model is shown in A (with ribbons) and B (without ribbons). The groups of residues engaged in hydrogen bonding interactions are as follows: [His 135<sup>6.64</sup>–Asn 139 (ECL<sub>1</sub>), Glu 145<sup>3.22</sup>–Lys 214 (ECL<sub>2</sub>) and Thr 216 (ECL<sub>2</sub>)], [Lys 214 (ECL<sub>2</sub>)–Gln 215 (ECL<sub>2</sub>) and His 228 (ECL<sub>2</sub>)], [Thr 207<sup>4.57</sup>–Tyr 211<sup>4.61</sup>], [Ser 320<sup>7.29</sup>–Gln 319 (ECL<sub>2</sub>)], [Tyr 156<sup>3.33</sup>–Tyr 326<sup>7.35</sup>]. (C and D) The hydrogen bonding interactions that are predicted to stabilize the central part of the PAR2 model is shown in C (with ribbons) and D (without ribbons). The groups of residues engaged in hydrogen bonding interactions are as follows: [Tyr 160<sup>3.37</sup>–Asn 303<sup>6.52</sup>], [Tyr 344<sup>7.53</sup>–Asn 93<sup>1.50</sup>], [Asn 93<sup>1.50</sup>–Asp 121<sup>2.50</sup>–Asp 340<sup>7.49</sup>–Asn 336<sup>7.45</sup>–Ser 337<sup>7.46</sup>–Asn 158<sup>3.35</sup>]. (E and F) The hydrogen bonding interactions that are predicted to stabilize the intracellular facing part of the PAR2 model is shown in E (with ribbons) and F (without ribbons). The groups of residues engaged in hydrogen bonding interactions are as follows: [Glu 278<sup>6.27</sup>–Lys 282<sup>6.31</sup>–Arg 281<sup>6.30</sup>], [Ser 277 (ICL<sub>3</sub>)–Asp 276 (ICL<sub>3</sub>)], [Glu 278 (ICL<sub>3</sub>)–Asp 276C (ICL<sub>3</sub>)] (the residues involved in hydrogen bond interaction are only shown for the sake of clarity). Hydrogen bonds are depicted as pink dashed lines with the bond length information. The residues involved in hydrogen bonding are rendered in ball and stick type. (For interpretation of the references to color in this figure legend, the reader is referred to the web version of this article.)

activation in some GPCRs. Agonist dependent movements of TM5 and TM6, involving residues Trp<sup>6.48</sup>, Phe<sup>6.44</sup>, Leu<sup>5.51</sup> Pro<sup>5.50</sup>, Ile/Leu<sup>3.40</sup> and Pro<sup>5.50</sup> was observed in the activation of GPCRs [94]. In protease activated receptors, the tryptophan residue in FxxCW<sup>6.48</sup>xP motif, is replaced by F<sup>6.48</sup>. Interestingly, in PAR2, apart from F<sup>6.48</sup> substitution, the F<sup>6.44</sup> residue is also substituted by Y 295<sup>6.44</sup>. In PAR2 Y<sup>6.44</sup>xxCF<sup>6.48</sup> motif hydrogen bonding interaction between Phe 299<sup>6.48</sup>, Asn 303<sup>6.52</sup> and Tyr 160<sup>3.37</sup> was observed (Fig. 8). We suggest that this interaction may give stability to the motif. Importantly, similar hydrogen bond was earlier identified as one of the important interactions, giving stability to the PAR1 structure [31]. Substitution of tryptophan to phenylalanine was shown to affect the structure, stability, and enzyme activity of the IIABMan subunit of the mannose transporter of *Escherichia coli* [95]. Further studies are needed to understand the implication of the substitution

of Trp<sup>6.48</sup> residue with Phe<sup>6.48</sup> in PARs. In the rhodopsin-like family, movement of TM3 and TM6 during the activation process has been identified [96,97]. It is possible that Tyr 295<sup>6.44</sup> may give additional stability through hydrophobic interactions. The other residues which were identified in GPCRs to play an important role in the activation process were Leu<sup>5.51</sup>, Ser<sup>5.42</sup>, Ser<sup>5.46</sup>, and Ile<sup>3.40</sup>; however, in PAR2 these residues were substituted by Ala<sup>5.51</sup>, Leu<sup>5.42</sup>, Leu<sup>5.46</sup> whereas Ile<sup>3.40</sup> is conserved, similar to β2AR and rhodopsin. The residues Leu<sup>5.42</sup>, Leu<sup>5.46</sup> were stabilized by

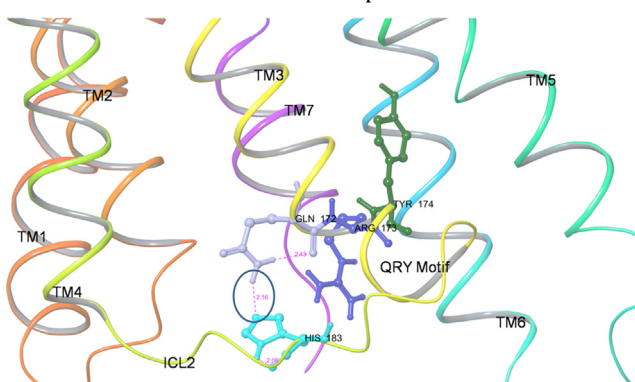


**Fig. 7.** QRY motif in PAR2 model. In PAR2, D<sup>3.49</sup>RY is replaced by QR<sup>3.50</sup>Y (172–174). The hydrogen bonding interaction between Gln 172<sup>3.49</sup>–His 183 (ICL<sub>2</sub>) is depicted by blue circle. Hydrogen bonds are shown with pink dashed lines. The orientation of Tyr 174<sup>3.51</sup> toward extracellular part is also shown. (For interpretation of the references to color in this figure legend, the reader is referred to the web version of this article.)

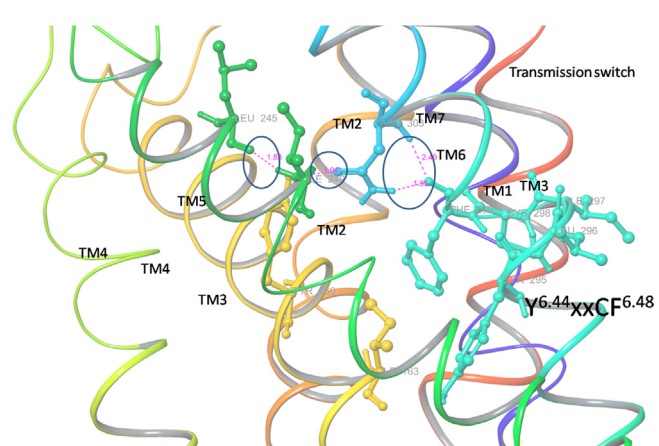


**Fig. 8.** Y<sup>6.44</sup>xxCF<sup>6.48</sup>xP<sup>6.50</sup> motif in PAR2 model. Hydrogen bonding interactions between residues Phe 299<sup>6.48</sup>, Asn 303<sup>6.52</sup> and Tyr 160<sup>3.37</sup> is depicted by pink dashed lines. The other residues which were identified to play an important role in the activation process in PAR1 were Leu<sup>5.51</sup>, Ser<sup>5.42</sup>, Ser<sup>5.46</sup>, and Ile<sup>3.40</sup>. However, in PAR2 these residues are substituted by Ala<sup>5.51</sup>, Leu<sup>5.42</sup>, Leu<sup>5.46</sup>, where Ile<sup>3.40</sup> is conserved between PAR1 and PAR2. The residues of this motif are displayed in ball and stick format and the hydrogen bonding interactions are highlighted with circles. (For interpretation of the references to color in this figure legend, the reader is referred to the web version of this article.)

hydrogen bonds. The effect of these substitutions on ligand activation and signaling needs to be investigated further. In dopamine D2 receptor, functional selectivity associated with Ser<sup>5.42</sup> to Ala and Ser<sup>5.46</sup> to Ala mutations were reported. Although, these mutations did not disrupt the overall conformation or signaling of the mutant receptors, they affected ligand activation [98]. Transmission switch was reported to link agonist binding site with the movement of TM5 and TM6 through rearrangement of the TM3-5-6 interface in some classes of GPCRs (as reviewed in [93]). Further studies may reveal the role of residue substitutions in PAR2 transmission switch and their effect on signaling.

### 3.5.4. Tyrosine toggle switch ( $DP^{7.50}xxY$ motif)

The NP<sup>7.50</sup>xxY motif, which is present toward the end of TM7 helix and is conserved in most of the GPCRs, is DP<sup>7.50</sup>xxY in PAR family and DP<sup>7.50</sup>FVY (340–344) in PAR2. Asp<sup>7.49</sup> was reported to be involved in extensive hydrogen bonding network with water molecules and a putative sodium ion ( $Na^+$ ). This sodium ion was termed as allosteric modulator and was reported to be involved in extensive hydrogen bonding with many residues of TM1 and TM2. Further, it was also observed that this sodium ion also interacts with a conserved Asp<sup>2.50</sup> in TM2 and Ser<sup>3.39</sup> in TM3, with two water molecules nearby [31]. It is interesting to observe similar interactions in PAR2 homology model also. In PAR2 homology model, Asp 340<sup>7.49</sup> and Tyr 344<sup>7.53</sup> showed extensive hydrogen bonding network mainly with conserved Asp 121<sup>2.50</sup> and Asp 93<sup>1.50</sup> respectively. Interestingly, Tyr 344<sup>7.53</sup> was seen to orient toward the extracellular surface in PAR2 while in other GPCRs Tyr 344<sup>7.53</sup> was positioned parallel to the lipid bilayer (Fig. 9). As mentioned in the earlier section, Asp 121<sup>2.50</sup> formed extensive network with various residues of TM1 and TM2 (refer Section 3.7). Tyr 344<sup>7.53</sup> was shown to play an important role in the activation of GPCRs as reviewed in Trzaskowski et al. [93]. Its in-swing along with Tyr<sup>5.58</sup> was known to bring about activation. Thus, it appears that in PAR2 the extensive bonding involving residues Asp121<sup>2.50</sup>, Asp 93<sup>1.50</sup> and Asp 336<sup>7.45</sup>, Tyr 345<sup>7.53</sup> may give rise to additional stability, which may explain tight regulation of PAR2 signaling.

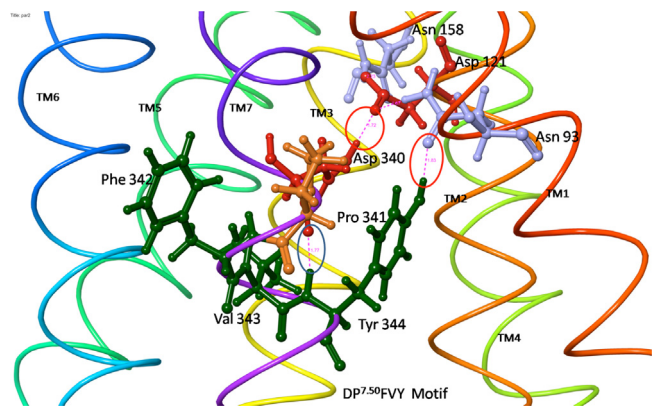


**Fig. 9.**  $DP^{7.50}$ FVY motif (Tyrosine toggle switch) of PAR2 model is illustrated. Hydrogen bonding interaction between Asp 340<sup>7.49</sup> of  $DP^{7.50}$ FVY motif and conserved Asp 121<sup>2.50</sup> is highlighted in a red circle. Hydrogen bonding interaction with Tyr 344<sup>7.53</sup> of  $DP^{7.50}$ FVY motif and Asn 93<sup>1.50</sup> is also shown in red circle. The hydrogen bonding between the residues of  $DP^{7.50}$ FVY motif namely Asp 340<sup>7.49</sup> and Tyr 344<sup>7.53</sup> is depicted with blue circle. A similar interaction centered around Asp<sup>2.50</sup> was observed in the PAR1 crystal structure also and was observed to play a key role in the activation of PAR1 [31]. Hydrogen bonding interactions are shown as pink dashed lines and the residues are displayed in ball and stick format. (For interpretation of the references to color in this figure legend, the reader is referred to the web version of this article.)

### 3.6. Prediction of binding cavity and difference between PAR1 and PAR2

Analysis of the PAR2 homology model and its comparison with the PAR1 crystal structure brings out interesting differences which may be useful in designing PAR2 specific drugs. The binding cavity of PAR2 appeared to be more open, possibly due to the absence of interactions between Tyr 183, His 255, Tyr 353, Asp 256 and Tyr 95, observed in PAR1 [31]. However, hydrogen bond interaction between His 228 (ECL<sub>2</sub>) and Gln 215 (ECL<sub>2</sub>) was observed. Further, extensive hydrogen bonding interaction between Gln 215 (ECL<sub>2</sub>), Lys 214 (ECL<sub>2</sub>), Thr 216 (ECL<sub>2</sub>) and Glu 145<sup>3.32</sup> (TM3) was

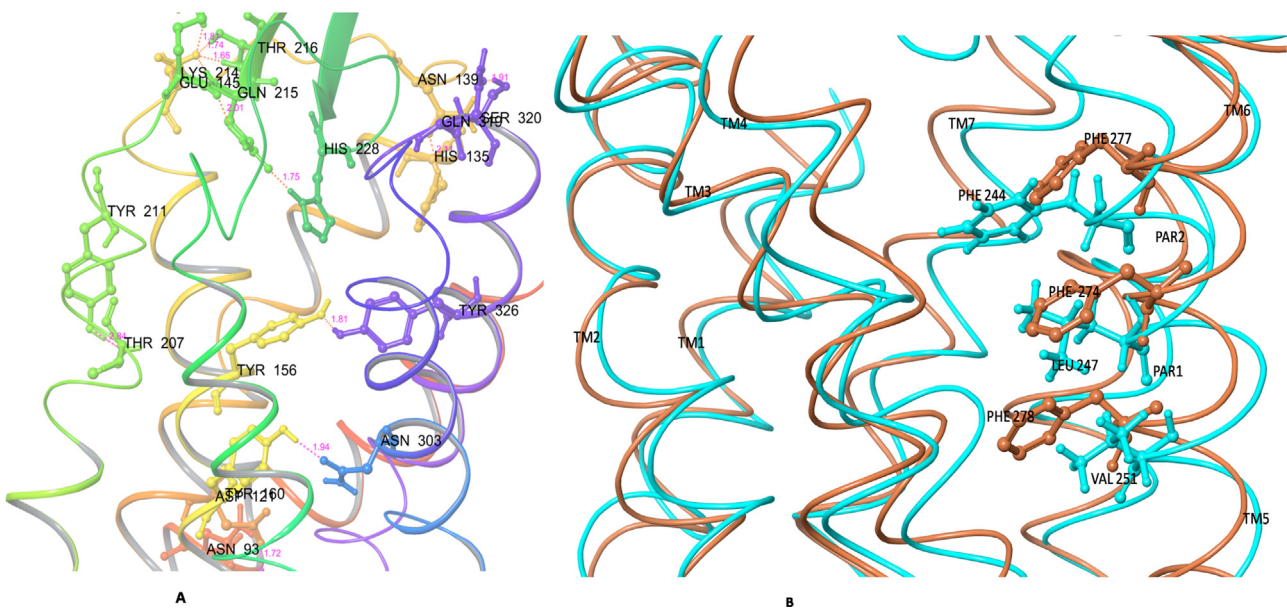


**Fig. 10.** (A) Predicted binding cavity in PAR2 model. The hydrogen bonding interactions involving residues His 228 (ECL<sub>2</sub>), Gln 215 (ECL<sub>2</sub>), Lys 214 (ECL<sub>2</sub>), Thr 216 (ECL<sub>2</sub>) and Glu 145<sup>3.32</sup> proposed to line the predicted binding cavity toward extracellular end of PAR2 model is depicted. Hydrogen bonding interactions between Tyr 156<sup>3.33</sup>–Tyr 326<sup>7.35</sup> and Tyr 160<sup>3.37</sup>–Asn 303<sup>6.52</sup>, that is proposed to form the base of the binding cavity is also shown. (B) Conformation of the residues Phe 244<sup>5.39</sup>, Leu 247<sup>5.42</sup> and Val 251<sup>5.46</sup> of PAR2 and comparison to corresponding residues in PAR1. The residues Phe 271<sup>5.39</sup>, Phe 274<sup>5.42</sup> and Phe 278<sup>5.46</sup> in PAR1 were substituted by Phe 244<sup>5.39</sup>, Leu 247<sup>5.42</sup> and Val 251<sup>5.46</sup> in PAR2 model. The conformation of these residues in the PAR2 model suggests that they may not give rise to substrate specificity. Hydrogen bonding interactions are shown as pink dashed lines and the residues involved are displayed in ball and stick format. (For interpretation of the references to color in this figure legend, the reader is referred to the web version of this article.)

**Table 2**

Receptors belonging to PAR phylogenetic cluster (Kakarala and Jamil [49]) and their ligand information based on GLIDA database.

S. no	Family of GPCR	Members of phylogenetic cluster with ligand information in GLIDA database	Ligand name, Pubchem ID and nature of the ligand
1.	Class A orphan receptor	GPR40.Human GPR17.Human CLTR1.Human (cysteinyl leukotrienes)	Linoleic acid (CID: 3931) agonist Oleic acid (CID: 965) agonist Aminolevulinic Acid (CID: 137) agonist BAYu9773 (CID: 5311015) Partial agonist LeukotrieneC4 (CID: 5283121) agonist Leukotriene D4 (CID: 6435286) agonist Leukotriene D4 (CID: 5280878) agonist Leukotriene E4 (CID: 5280879) agonist Cinaleukast (CID: 6436135) antagonist Zafireukast (CID: 5717) antagonist Amlexanox (CID: 2161) antagonist Montelukast (CID: 5281040) antagonist RG 12525 (CID: 29044) antagonist Nedocromil (CID: 50294) antagonist
2.	Putative/unclassified Class A receptor	Q9Y2T6.Human	CP55940 (CID: 5311056) Agonist
3.	Platelet activating factor receptor	PAFR.Human	Pantoic acid (CID: 439251) Full Agonist Brotizalam (CID: 2451) Antagonist Triazolam (CID: 5556) Antagonist AABT 491(CID: 154086) Antagonist
4.	Purinoceptors	P2Y14.Human  P2Y12.Human	Uridine diphosphate galactose (CID: 18068) full agonist UDP-N-acetylglucosamine (CID: 439157) agonist Uridine diphosphate glucuronic acid (CID: 17473) full agonist 2-Methylthio-ADP methylthio-ADP (CID: 121990) full agonist Epoprostenol (CID: 5280427) agonist Adenosine 5'-O-(3-thiotriphosphate) alpha-thioadenosine triphosphate (CID: 440317) full agonist Clopidogrel (CID: 60606) antagonist Ticlopidine (CID: 5472) antagonist

observed in PAR2. The other important interactions, which may give rise to subtype specificity, is between Tyr 156<sup>3,33</sup>–Tyr 326<sup>7,35</sup> and Tyr 160<sup>3,37</sup>–Asn 303<sup>6,52</sup>. These interactions may also give rise to additional stability to TM3, TM6 and TM7 (Fig. 10A). Zhang et al. reported that the residues Phe 271, Phe 274 and Phe 278 may give subtype specificity in PAR1 [31]. Interestingly, these residues were substituted by Phe 244<sup>5,39</sup>, Leu 247<sup>5,42</sup> and Val 251<sup>5,46</sup> in PAR2. Analysis of PAR2 model showed that Phe 244<sup>5,39</sup> may play an important role in ligand binding, as it is positioned much deeper into the binding cavity. Although the effect of phenylalanine to leucine substitution is not evident from our studies, it is possible

that this substitution may result in more stabilized inactive conformation [99]. The other interactions which might be important for ligand binding are the one between Ser 320<sup>7,29</sup>–Gln 319 (ECL<sub>3</sub>) and His135 (ECL<sub>1</sub>)–Asp 139 (ECL<sub>1</sub>), Thr 207<sup>4,57</sup> and Tyr 211<sup>4,61</sup>.

### 3.7. Binding affinity studies of PAR2 model with putative ligands identified from phylogenetic clustering of GPCRs

Based on the published article on phylogenetic classification of Class A rhodopsin GPCRs by our group, protease activated receptors were shown to cluster with GPCRs like purinoceptors, platelet

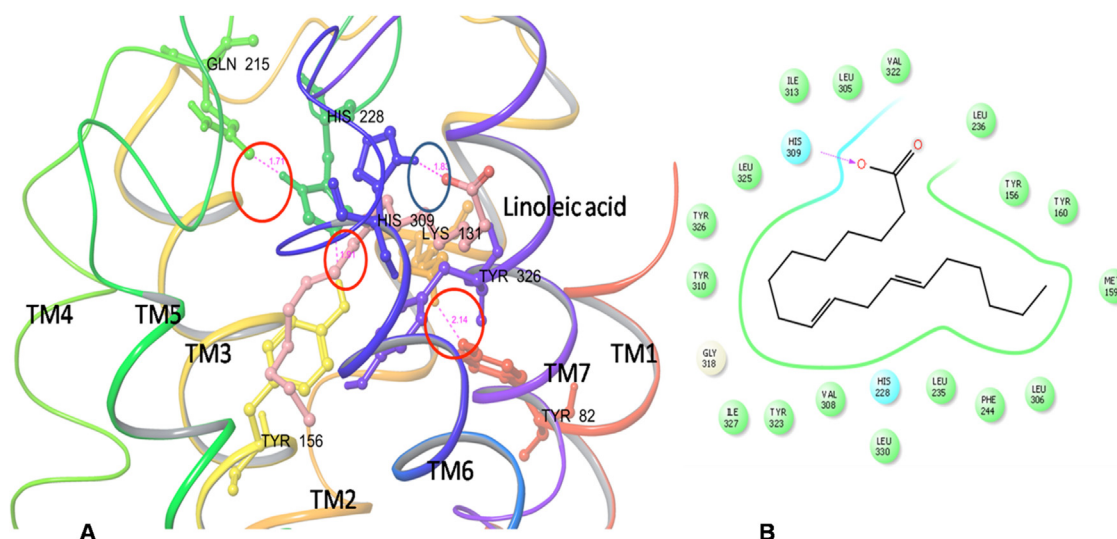


**Fig. 11.** (A) Binding pose of PAR2 model-linoleic acid complex. Binding pose of linoleic acid shows that it forms hydrogen bond with His 309<sup>6,58</sup>, highlighted with blue circle. Post docking interactions between Tyr156<sup>3,33</sup>, His 228 (ECL<sub>2</sub>) and Tyr 82<sup>1,39</sup> and Lys 131<sup>2,60</sup> and the interaction between His 228 (ECL<sub>2</sub>) and Gln 215 (ECL<sub>2</sub>) observed in the apoprotein are depicted within red circles. The hydrogen bond interaction is indicated by pink dashed lines and the residues involved in hydrogen bonding interactions are displayed in ball and stick format. (B) LigPlot interaction map of PAR2 model-linoleic acid. LigPlot map depicting the hydrogen bond interaction of His 309<sup>6,58</sup> with linoleic acid in PAR2 is shown. The hydrogen bond interactions are indicated by pink arrow. (For interpretation of the references to color in this figure legend, the reader is referred to the web version of this article.)

**Table 3**

Binding affinity analysis of putative ligands with PAR2 homology model. Glide score, IFD score and Prime/MMGBSA dG bind values of ligands (agonists and antagonist) along with the interacting residues is given. The ligands for which MDS studies were undertaken are shown in bold.

S. no	Ligands, Pubchem ID, agonist/antagonist	Glide score	IFD score	PRIME/MMGBSA dG bind	Interacting residues
1.	Linoleic acid (CID: 3931) Agonist	−8.760	−554.128	−111.016	His 309 (TM6)
2.	<b>Oleic acid (CID: 965)</b> Agonist	<b>−10.948</b>	<b>−550.780</b>	<b>−107.328</b>	<b>Lys 131 (TM2)</b>
3.	Aminolevulinic acid (CID: 137) Agonist	−6.348	−545.641	−35.12	Leu 236 (ECL <sub>2</sub> ), Leu 235 (ECL <sub>2</sub> ), Tyr 310 (TM6), Gln 234 (ECL <sub>2</sub> ), Tyr 326 (TM7).
4.	<b>CP55940 (CID: 5311056)</b> Agonist	<b>−13.815</b>	<b>−556.264</b>	<b>−127.577</b>	<b>π–π interaction with His228 (ECL2), hydrogen bonding interaction with His 228 (ECL<sub>2</sub>), Lys131 (TM2) and Ile 327 (TM7)</b>
5.	BAYu9773 (CID: 5311015) Partial agonist	−10.378	−410.268	−126.50	Ser 316 (ECL <sub>3</sub> ), Gly 318 (ECL <sub>3</sub> ), Gln 317 (ECL <sub>3</sub> ), Gln 319 (ECL <sub>3</sub> ), Val 230 (ECL <sub>2</sub> )
6.	Leukotriene C4 (CID: 5283121) Agonist	−9.913	−412.547	−97.840	Lys 315 (ECL <sub>3</sub> ), Leu 231(ECL <sub>2</sub> )
7.	<b>Leukotriene D4 (CID: 6435286)</b> Agonist	<b>−12.200</b>	<b>−409.652</b>	<b>−126.479</b>	<b>Lys 315 (ECL<sub>3</sub>), Gln 317 (ECL<sub>3</sub>), Gln 234 (ECL<sub>2</sub>), Gly 238 (ECL<sub>2</sub>)</b>
8.	Leukotriene D4 (CID: 5280878) Agonist	−12.200	−409.652	−126.50	Gln317 (ECL <sub>3</sub> ), Gly 238 (ECL <sub>2</sub> )
9.	Leukotriene E4 (CID: 5280879) Agonist	−9.108	−403.643	−104.678	Gln 234 (ECL <sub>2</sub> ), Glu 233 (ECL <sub>2</sub> ), Gly 238 (ECL <sub>2</sub> ), Lys 315(ECL <sub>3</sub> )
10.	Cinaleukast (CID: 6436135) Antagonist	−9.480	−400.155	−102.379	Gln 317(ECL <sub>3</sub> )
11.	Zafirleukast (CID: 5717) Antagonist	−11.955	−405.081	−115.574	Gln 317(ECL <sub>3</sub> ),His 309 (TM6), Leu236 (ECL <sub>2</sub> )
12.	Amlexanox (CID: 2161) Antagonist	−9.276	−398.422	−83.771	Leu 236 (ECL <sub>2</sub> ), Pi interaction with His 309 (TM6), Phe 241(TM5)
13.	<b>Montelukast (CID: 5281040)</b> Antagonist	<b>−10.924</b>	<b>−403.062</b>	<b>−135.483</b>	<b>Gly 238 (ECL<sub>2</sub>), Gln 234 (ECL<sub>2</sub>), Gln317 (ECL<sub>3</sub>), π–π interaction with Tyr 310 (TM6) and Tyr 323 (TM7)</b>
14.	RG 12525 (CID: 129044) Antagonist	−9.285	−393.576	−104.32	Tyr 310 (TM6) and Tyr 323 (TM7), Leu 235(ECL <sub>2</sub> ), Gln 234 (ECL <sub>2</sub> ). <b>π–π interaction with Tyr 310 (TM6)</b>
15.	Pantoic acid (CID: 439251) Full agonist	−8.132	−383.828	−29.143	Gln 234 (ECL <sub>2</sub> ), Leu 236 (ECL <sub>2</sub> ), Leu 235(ECL <sub>2</sub> )
16.	Brotizalam (CID: 2451) Antagonist	−10.748	−552.141	−118.082	Leu 235 (ECL <sub>2</sub> ), π–π interaction with Tyr 326 (TM7) and His 228 (ECL <sub>2</sub> )
17.	Triazolam (CID: 5556) Antagonist	−7.433	−547.110	−90.653	Leu 235 (ECL <sub>2</sub> ), π–π interaction with Phe 244(TM5) and Tyr 326(TM7)
18.	<b>AABT 491 (CID: 154086)</b> Antagonist	<b>−10.501</b>	<b>−399.561</b>	<b>−125.719</b>	<b>Leu 235 (ECL<sub>2</sub>), Leu 236 (ECL<sub>2</sub>), Gln234 (ECL<sub>2</sub>) and π–π interaction with Tyr156 (TM3), Phe 244 (TM5)</b>
19.	<b>Uridine diphosphate galactose (CID: 18068)</b> Full agonist	<b>−9.574</b>	<b>−549.962</b>	<b>−75.614</b>	<b>Gln 234(ECL<sub>2</sub>), Tyr 326 (TM7), Tyr 310 (TM6)</b>
20.	UDP-N-acetylglucosamine (CID: 439157) Agonist	−7.246	−547.470	−61.951	Gly 238 (ECL <sub>2</sub> ), Gln 317(ECL <sub>3</sub> ) and Gln234 (ECL <sub>2</sub> )

Table 3 (Continued)

S. no	Ligands, Pubchem ID, agonist/antagonist	Glide score	IFD score	PRIME/MMGBSA dG bind	Interacting residues
21.	Uridine diphosphate glucuronic acid (CID: 17473) Full agonist	-10.001	-548.441	-57.30	Lys 315 (ECL <sub>3</sub> ), Gln 234 (ECL <sub>2</sub> ), Leu 231 (ECL <sub>2</sub> ), Gly 318 (ECL <sub>3</sub> ), Ser 320 (ECL <sub>3</sub> ), Tyr 326 (TM7), Gly 238 (ECL <sub>2</sub> )
22.	2-methylthio-ADP methylthio-ADP (CID: 121990) Full agonist	-8.012	-550.019	-72.90	Gln 317 (ECL <sub>3</sub> ), Lys 315 (ECL <sub>3</sub> ), Gly 238 (ECL <sub>2</sub> ), Glu 233 (ECL <sub>2</sub> ). π–π bond interaction with Tyr 310 <sup>6,49</sup>
23.	Epoprostenol (CID: 5280427) Agonist	-12.969	-558.352	-110.134	Tyr 82 (TM1), Leu 236 (ECL <sub>2</sub> ), Lys 131 (TM2), Asp 229 (ECL <sub>2</sub> ), Tyr 156 (TM3)
24.	Adenosine 5'-O-(3-thiotriphosphate) alpha-thioadenosine triphosphate (CID: 440317) Full agonist	-11.374	-553.766	-65.307	Gln 317 (ECL <sub>3</sub> ), Leu 235 (ECL <sub>2</sub> ), Tyr 323 (TM7), Tyr 156 (TM3), π–π interaction with Tyr 310 (TM6)
25.	<b>Clopidogrel (CID: 60606) Antagonist</b>	<b>-11.562</b>	<b>-555.110</b>	<b>-113.88</b>	<b>Leu 235 (ECL<sub>2</sub>) and Leu 236 (ECL<sub>2</sub>) and with π–π interactions between Phe 244 (TM5), His 228 (ECL<sub>2</sub>) and Tyr 323 (TM7)</b>
26.	Ticlopidine (CID: 5472) Antagonist	-9.951	-550.556	-105.995	π–π interaction with Tyr 156 (TM3) and Phe 244 (TM5) and His 309 (TM6) bonding interaction with Tyr 326 (TM7)

activating factor, Class A orphan and putative/unclassified Class A receptors [49]. Phylogenetic clustering was useful in the identification of the chemical nature of ligand binding to orphan GPCR and other classes of GPCRs [100–103]. Thus, we used the same principle to identify putative ligands for PAR2 as there are no endogenous ligands known for PAR2. We obtained the ligand information of these receptors from GLIDA database [50] and investigated the binding affinity of some of the ligands of these receptors with the PAR2 homology model. The information of the receptors belonging to PAR cluster along with their ligand information (GLIDA database) is given in Table 2.

### 3.7.1. Binding affinity and molecular dynamics studies with agonists and antagonist of receptors, which clustered with protease activated receptors

3.7.1.1. Ligands belonging to Class A orphan receptors. GPR40 – linoleic acid and oleic acid. Linoleic acid and oleic acid act as agonist for the Class A orphan receptor GPR40. Interestingly, linoleic acid and oleic acid act as agonist for other receptors like GPR119, GPR84, GPR120, GPR43 (FFAR2) and GPR41 (FFAR3) [104]. Binding affinity studies using IFD and Prime/MMGBSA method showed that linoleic acid and oleic acid indicate promising binding affinity with PAR2 (Table 3). Further, the analysis of docking pose and

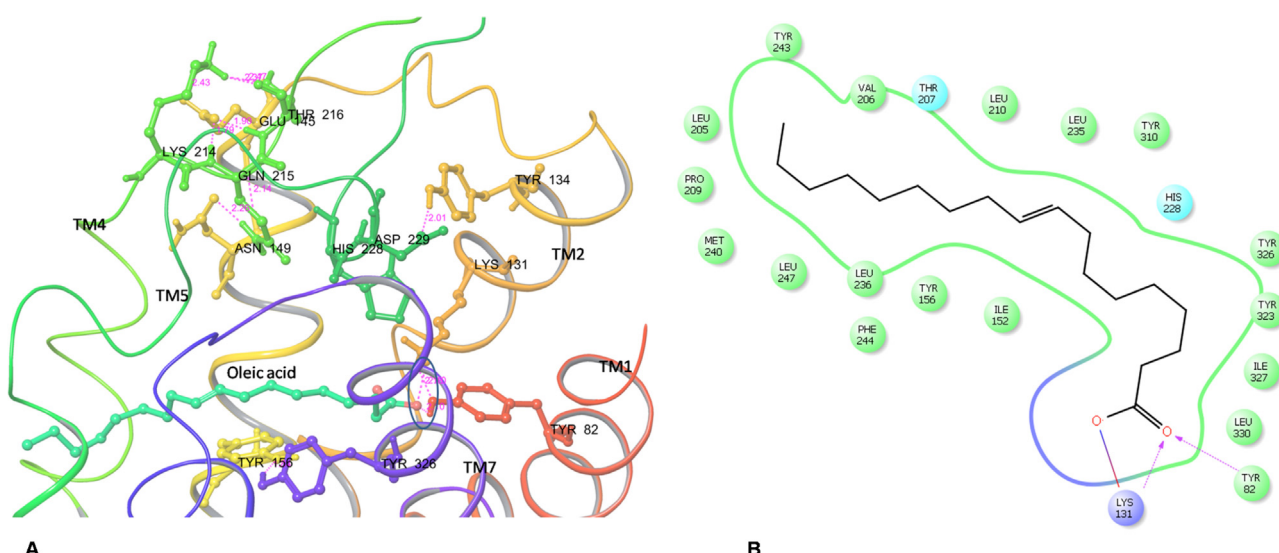


**Fig. 12.** (A) Binding pose of PAR2 model-oleic acid complex. Binding pose of oleic acid shows that it was stabilized by hydrogen bonding interactions with Tyr 82<sup>1,39</sup> and salt bridge interaction of Lys 131<sup>2,60</sup> (highlighted with blue circle). The other hydrogen bond interactions are indicated by pink dashed lines and the residues involved in hydrogen bonding interactions are displayed in ball and stick format. (B) LigPlot interaction map of PAR2-oleic acid complex. LigPlot map depicting hydrogen bond interaction between Tyr 82<sup>1,39</sup> and salt bridge interaction of Lys 131<sup>2,60</sup> with oleic acid in PAR2 model. The hydrogen bond is depicted by pink arrow and salt bridge by a pink line. (For interpretation of the references to color in this figure legend, the reader is referred to the web version of this article.)

the interactions in the docked complex (PAR2-linoleic acid) brings out important observations that indicate the possible direction of movement in the transmembrane helices with the docking of linoleic acid. We propose that docking of linoleic acid, was facilitated by disruption of hydrogen bonds between Tyr 156<sup>3,33</sup>–Tyr 326<sup>7,35</sup> (ECL<sub>2</sub>), which was predicted as one of the stabilizing interactions in PAR2 model (described in Section 3.5). This prediction was based on the observed increase in the distance between Tyr 156<sup>3,33</sup> and Tyr 326<sup>7,35</sup> to 6.79 Å after docking. The best docked pose analysis showed hydrogen bond interaction between linoleic acid and His 309<sup>6,58</sup> in PAR2 model (Fig. 11A and B).

The analysis of the selected binding pose of oleic acid with PAR2 shows hydrogen bond interaction with Tyr 82<sup>1,39</sup> and a salt bridge interaction with Lys 131<sup>2,60</sup>. Docking of oleic acid appears to have disrupted stabilizing interactions between His 228 (ECL<sub>2</sub>) and Gln 215 (ECL<sub>2</sub>) (1.75–3.75 Å) (refer Section 3.6). Gln 215 (ECL<sub>2</sub>) was observed to form new hydrogen bonding interaction with Asn 149<sup>3,26</sup> (Fig. 12A and B) after docking. Molecular dynamics studies of PAR2-oleic acid complex for 5 ns showed stable hydrogen bond interaction with Lys 131<sup>2,60</sup> (refer Section 2.2) (Movie M1).

Further experimental studies are required to prove the binding affinity of these fatty acids and their effects on PAR2 signaling in breast cancer. Interestingly, oleate was reported to stimulate proliferation of breast cancer cells via GPR40 [105]. Importantly, high levels of dietary fat intake was shown to increase the risk of breast cancer, promote proliferation of breast cancer cell and enhance metastasis [104,105]. Thus, the promising binding affinity of linoleic and oleic acid with PAR2 might suggest a possible mechanism that explains the correlation between high circulating fatty acids in normal as well as in obese women and breast cancer. Moreover, the stable PAR2 receptor-oleic acid complex (Movie M2) suggests the possibility of these fatty acids activating both GPR40 and PAR2, resulting in enhanced activation of downstream signaling cascade and stimulation of breast cancer cells. It would be interesting to check the PAR2 activity and circulating fatty acids in breast cancer patients.

*GPR17 – aminolevulinic acid.* In our study, aminolevulinic acid, the ligand of GPR17, showed less binding affinity (Table 3). However, it is interesting to note that GPR17 showed cross-reactivity with P2Y and cysteinyl leukotriene receptor ligands [106], suggesting that endogenous ligands of the receptors belonging to this cluster may cross react.

*Cysteinyl leukotriene receptors:* CLTR1\_Human – BAYu9773, leukotriene C4, leukotriene D4, leukotriene E4, cinalukast, zafirlukast, amlexanox, montelukast & RG 1252. CLTR2\_Human – nedocromil. Cysteinyl leukotriene receptors belong to the Class A orphan receptors and play an important role in signaling pathophysiology of inflammatory diseases and inflammatory processes (reviewed by Singh et al. [107]). Cysteinyl leukotriene receptor 1 (CLTR1\_Human) and cysteinyl leukotriene receptor 2 (CLTR2\_Human) represent two subgroups of cysteinyl leukotriene receptors.

The agonists (endogenous) of cysteinyl leukotriene receptors namely, LTC4, LTD4, LTE4, were studied for the binding affinity with PAR2 model. Induced fit docking analysis, Prime/MMGBSA analysis and molecular dynamics simulation studies gave useful insights regarding binding affinity of these agonists with PAR2. Among the different classes of leukotrienes studied, leukotriene D4 (LTD4), showed a promising binding affinity in comparison to leukotriene C4 and E4 (Table 3).

Analysis of the binding pose of LTD4 indicated that docking of LTD4 led to the disruption of the hydrogen bond between Tyr 156<sup>3,33</sup> and Tyr 326<sup>7,35</sup> (one of predicted stabilizing interaction in PAR2, Section 3.5). Interestingly, the new hydrogen bonding interaction between Tyr 156<sup>3,33</sup> and His 228 (ECL<sub>2</sub>) was observed (Fig. 13A and B) in the post docking stage, suggesting movement of TM3 in the docking process. LTD4 was stabilized by hydrogen bonding interactions between Gln 234 (ECL<sub>2</sub>), Gly 238 (ECL<sub>2</sub>), Lys 315 (ECL<sub>3</sub>) and Gln 317 (ECL<sub>3</sub>) respectively. The results obtained in our study suggest that leukotrienes may interact with PAR2 by binding to loop region. Superficial interaction of leukotriene D4 may lead to the activation of GPCRs; leukotriene D4 may bind in a sequential manner, starting from extracellular loops and penetrating deep down with the formation of various conformational intermediates. This mechanism was proposed for tethered agonist peptide activation in PAR1 [31]. Molecular dynamics simulation studies of PAR2-LTD4 complex showed stable hydrogen bonding interactions with Gln 234 (ECL<sub>2</sub>), Lys 315 (ECL<sub>3</sub>) and Gln 317 (ECL<sub>3</sub>) in most of the frames (Movie M3).

Although, leukotrienes were predicted to be able to activate other receptor classes such as purinergic receptors P2Y12 and leukotriene B4 receptors (as reviewed by Bäck et al. [108]), this is the first *in silico* study that suggests that LTD4 may bind to PAR2. Our prediction of high binding affinity of LTD4 with PAR2

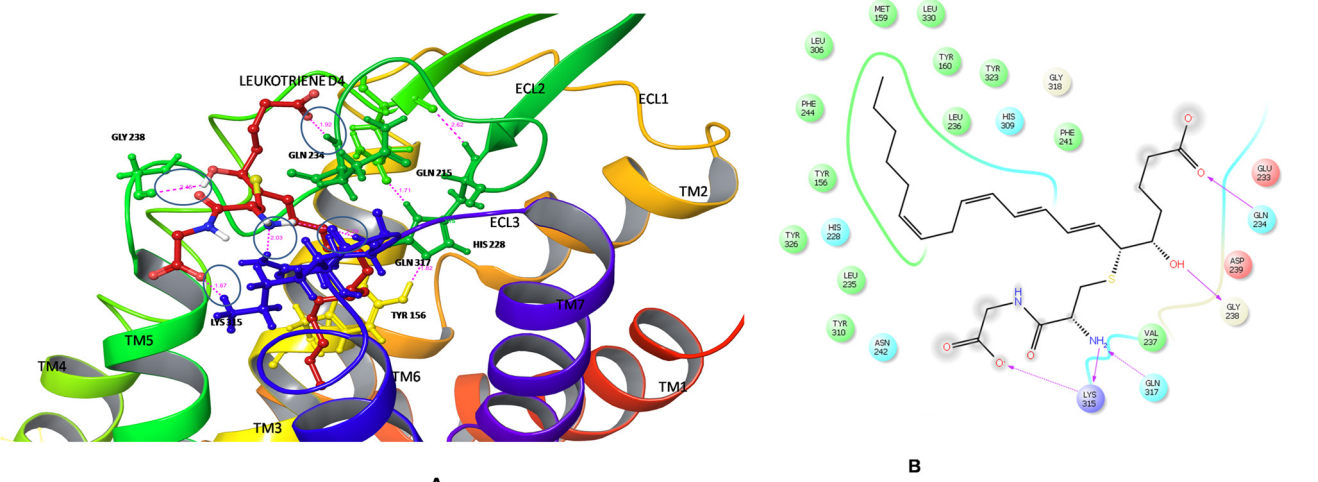


**Fig. 13.** (A) Binding pose of PAR2 model-leukotriene D4 complex. Binding pose of leukotriene D4 shows that it is stabilized by hydrogen bonding interactions with Gln 234 (ECL<sub>2</sub>), Gly 238 (ECL<sub>2</sub>), Lys 315 (ECL<sub>3</sub>), and Gln 317 (ECL<sub>3</sub>) (highlighted with blue circle). The hydrogen bond interaction is indicated by pink dashed lines and the residues involved in hydrogen bonding interactions are displayed in ball and stick format. (B) Ligand interaction map of PAR2 model-leukotriene D4 complex. LigPlot map depicting hydrogen bond interactions between leukotriene D4 and Gln 234 (ECL<sub>2</sub>), Gly 238 (ECL<sub>2</sub>), Lys 315 (ECL<sub>3</sub>) and Gln 317 (ECL<sub>3</sub>) of PAR2 model. The hydrogen bond interactions are depicted by pink arrows.

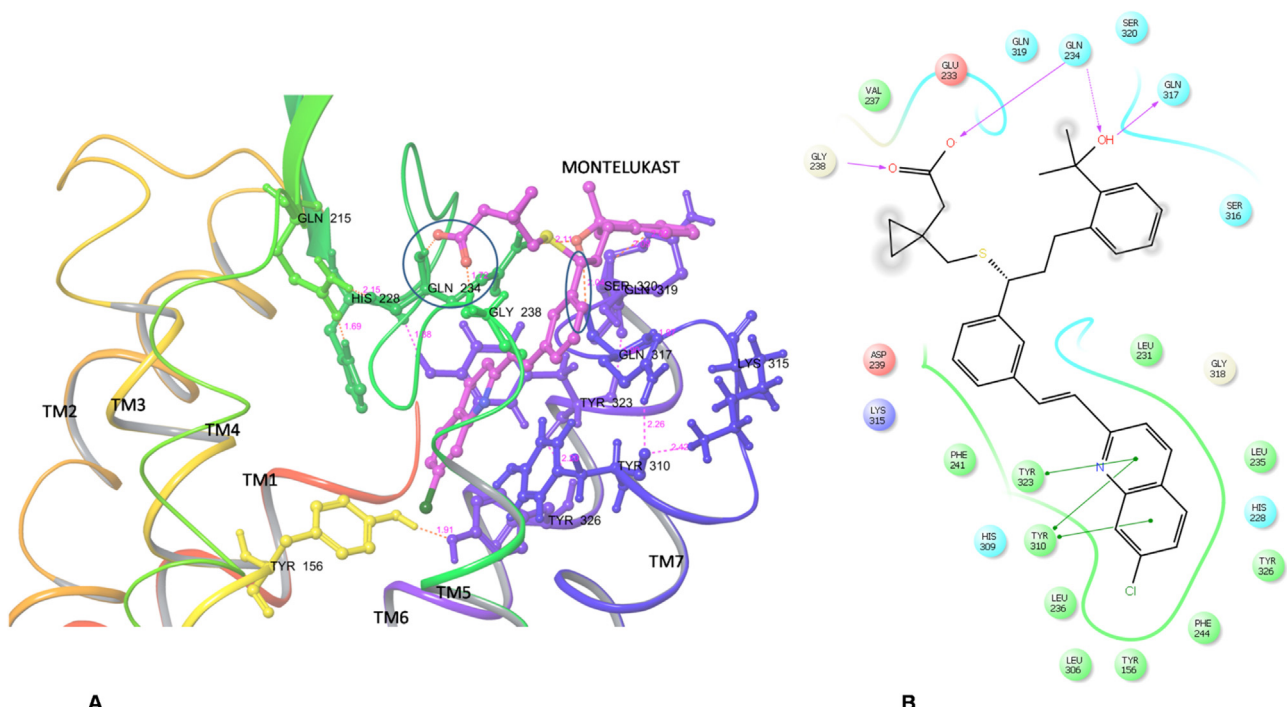


**Fig. 14.** (A) Binding pose of PAR2 model-montelukast complex. Binding pose of montelukast shows that it is stabilized by hydrogen bond interactions with Gln 234 (ECL<sub>2</sub>), Gly 238 (ECL<sub>2</sub>) and Gln 317 (ECL<sub>3</sub>) of PAR2 model (highlighted with blue circle). The hydrogen bond interactions are indicated by pink dashed lines and the residues involved in hydrogen bonding interactions are displayed in ball and stick format. (B) Ligand interaction map of PAR2 model-montelukast complex. LigPlot map showing hydrogen bond interactions between montelukast-Gln 234 (ECL<sub>2</sub>), Gly 238 (ECL<sub>2</sub>) and Gln 317 (ECL<sub>3</sub>) residues of PAR2 model is depicted. The hydrogen bonding is depicted by pink arrows and  $\pi-\pi$  interaction with Tyr 310<sup>6,59</sup> and Tyr 323<sup>7,32</sup> with montelukast is depicted by green lines. (For interpretation of the references to color in this figure legend, the reader is referred to the web version of this article.)

explains the experimental finding that reported delay in the onset of inflammation in protease activated receptor 2-deficient mice [109]. Thus, it is possible that LTD4 may activate both CLTR1\_Human and PAR2, escalating the signaling process involved in breast cancer. This mechanism may also explain the role of pro-inflammatory cysteinyl leukotriene receptors in breast tumor tissue, leading to tumor progression [110]. Interestingly, low CLTR1 receptor expression together with high CLTR2 expression levels was suggested to be useful parameters in the prognosis and treatment of breast cancer patients [110].

The antagonists of the CLTR1\_Human and CLTR2\_Human namely cinaleukast, zafirleukast, amlexanox, montelukast and nedocromil were also studied for their binding affinity with the PAR2 model. The order of their binding affinity obtained in this study was as follows; montelukast > zafirleukast > RG 12525 > cinaleukast > amlexanox (Table 3).

Among these antagonists, montelukast showed high affinity ( $-135$  Kcal/mol) in comparison to other antagonists investigated (Table 3). The binding pose of montelukast showed that it was stabilized through hydrogen bond interaction with Gln 234 (ECL<sub>2</sub>), Gly 238 (ECL<sub>2</sub>), Gln 317 (ECL<sub>3</sub>) and  $\pi-\pi$  interactions with residues Tyr 310<sup>6,59</sup> and Tyr 323<sup>7,32</sup>.

Tyr 310<sup>6,59</sup> is shown to interact by hydrogen bond with Gln 317 (ECL<sub>3</sub>) and Lys 215 (ECL<sub>2</sub>) (Fig. 14A and B). The docked position of montelukast appeared to be stabilized with hydrogen bond interaction between Tyr 156<sup>3,33</sup>-Tyr 326<sup>7,35</sup> at the base of binding cavity and interactions between several residues; Tyr 326<sup>7,35</sup>-Tyr 323<sup>7,32</sup>, Tyr 310<sup>6,59</sup>-Lys 315 (ECL<sub>3</sub>) and Tyr 323<sup>7,32</sup>-His228 (ECL<sub>2</sub>) respectively (Fig. 14A and B). The molecular dynamics simulation study showed stable interaction of montelukast with Gln 317 (ECL<sub>3</sub>) and Gln 234 (ECL<sub>2</sub>) (Movie M6). It is important to note that binding pose of montelukast was similar to that of leukotriene D4, i.e. binding site was located close to the loops. Interestingly antagonist of

CLTR2\_Human, nedocromil (CID: 50294) failed to bind with PAR2 receptor under conditions used in this study.

**3.7.1.2. Ligands belonging to putative/unclassified Class A orphan receptor, Q9Y2T6\_Human – CP55940.** CP55940 a synthetic cannabinoid structurally related to phytocannabinoid  $\Delta 9$ -tetrahydrocannabinol (THC) is the cognate ligand for Q9Y2T6\_Human, a putative/unclassified Class A receptor. Binding affinity study of CP55940 with PAR2 model showed a promising binding affinity (Table 3). Interestingly, the free energy of ligand binding calculated by Prime/MMGBSA was similar to leukotriene D4 (Table 3). The best docking pose selected showed hydrogen bond interactions of CP55940, with His 228 (ECL<sub>2</sub>), Asp 229 (ECL<sub>2</sub>), Lys 131<sup>2,60</sup> and Ile 327<sup>7,36</sup> (Fig. 15A and B). Molecular dynamics simulation study of PAR2-CP55940 complex, showed hydrogen bonding interaction with residues Lys 131<sup>2,60</sup> and Ile 327<sup>7,30</sup> in most of the frames (Movie M4). Interestingly, CP55940 binding site was different when compared to that of leukotriene D4, while the former was positioned inside the binding cavity, the latter showed superficial interaction pertaining to loop regions.

Although, CP55940 was identified as an agonist for putative/unclassified Class A receptor experimental evidences have reported antagonist action of synthetic cannabinoids. Importantly, synthetic cannabinoids were shown to modulate the cyclooxygenase-2 (COX-2) signaling pathway by inhibiting the activity of the downstream molecules c-Fos, c-Jun, and Cdc42 in breast cancer cells [111]. Interestingly, recent investigations have reported the beneficial effects of cannabinoids in the treatment of breast cancer [112]. Importantly, studies proved the binding affinity of synthetic cannabinoids to additional receptors such as the vanilloid receptor 1 (TRPV1) and GPR55 (Class A orphan GPCR) [113]. Thus, CP55940 may act as an antagonist to PAR2, thereby inhibiting the signaling cascade leading to the development of breast cancer.

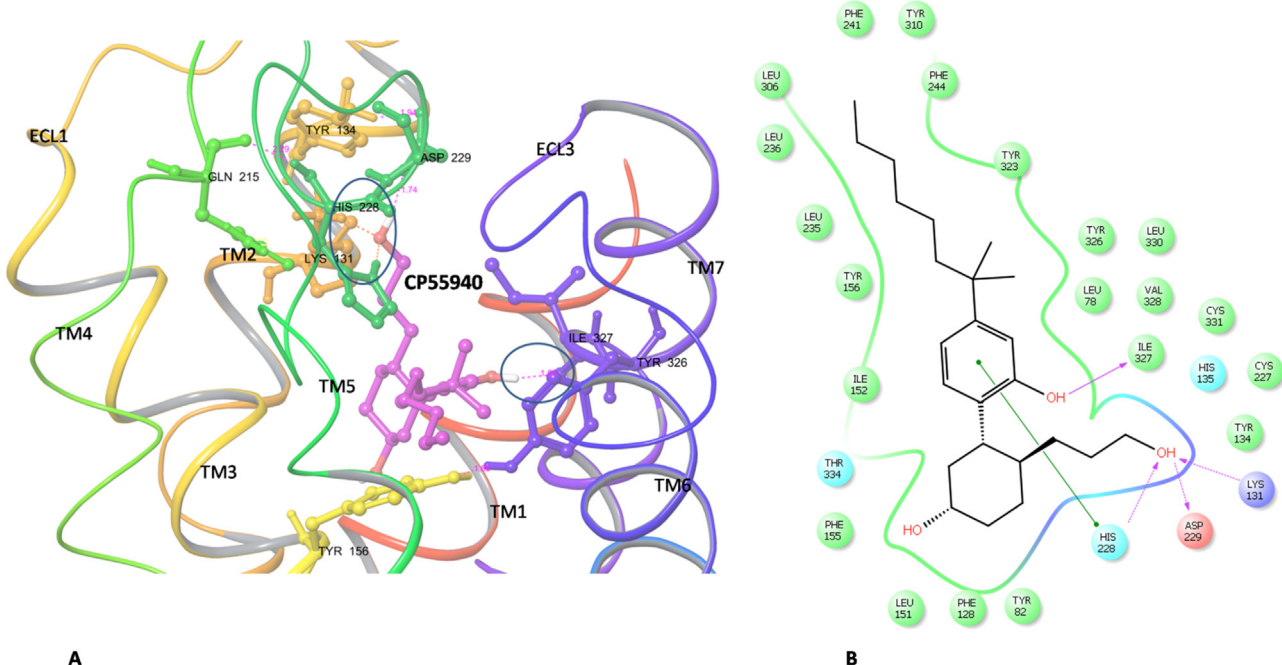


**Fig. 15.** (A) Binding pose of PAR2 model-CP55940 (phytocannabinoid) complex. Binding pose of CP55940 shows that it is stabilized by hydrogen bond with His 228 (ECL<sub>2</sub>), Asp 229 (ECL<sub>2</sub>), Lys 131 (ECL<sub>2</sub>), Ile 327 (ECL<sub>2</sub>) residues of PAR2 model (highlighted with blue circle). The hydrogen bond interactions are indicated by pink dashed lines and the residues involved in hydrogen bonding interactions are displayed in ball and stick format. (B) LigPlot interaction map of PAR2 model-CP55940 (phytocannabinoid) complex. LigPlot diagram depicting hydrogen bond interactions between CP55940 and His 228 (ECL<sub>2</sub>), Asp 229 (ECL<sub>2</sub>), Lys 131 (ECL<sub>2</sub>), and Ile 327 (ECL<sub>2</sub>). The hydrogen bond interactions are indicated by pink arrows and π-π interaction in green lines. (For interpretation of the references to color in this figure legend, the reader is referred to the web version of this article.)

Further experimental studies on the binding affinity may prove useful in analyzing its therapeutic efficacy against of CP55940 in breast cancer.

**3.7.1.3. Ligands belonging to platelet activating factor receptor. PAFR\_Human – pantoic acid, brotizalam, triazolam, AABT 491.** Platelet-activating factor receptor (PAFR) is involved in inflammation, oncogenic transformation, tumor growth, angiogenesis and

metastasis [114]. Pantoic acid, brotizalam, triazolam, AABT 491 are some of the known ligands of the receptor PAFR\_Human. Interestingly, pantoic acid, a full agonist of PAFR showed low free energy of ligand binding (PRIME/MMGBSA) with PAR2 model, suggesting its low affinity (**Table 3**).

The results of the docking study of the antagonists of PAFR suggest promising binding affinity to AABT 491 and brotizalam in comparison to triazolam (**Table 3**).

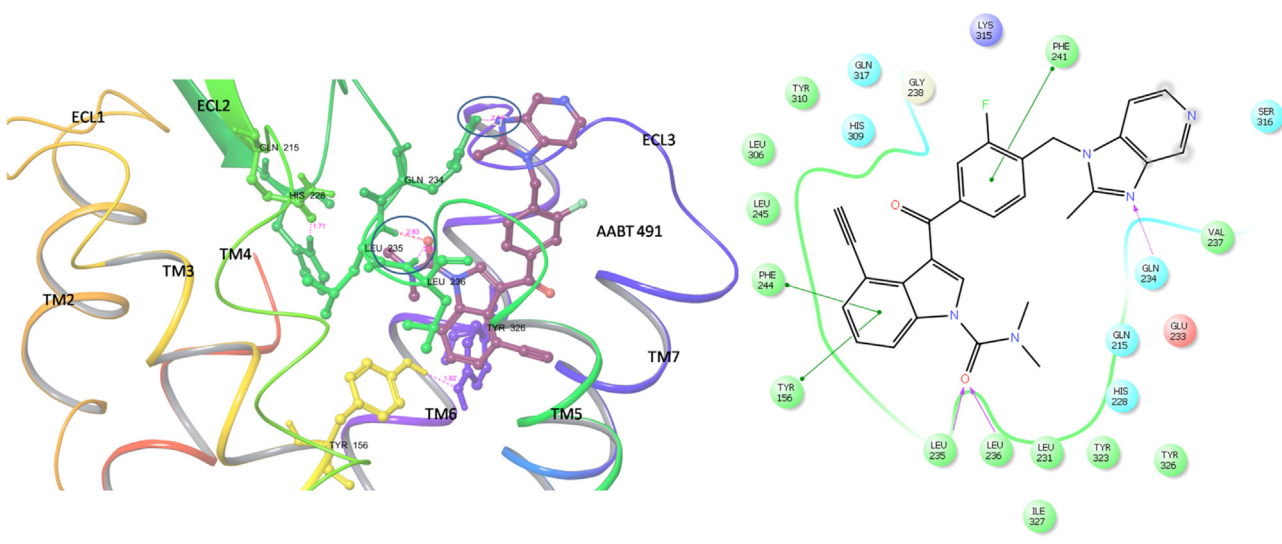


**Fig. 16.** (A) Binding pose of PAR2 model-AABT491 complex. Binding pose of AABT491 shows that it forms hydrogen bond with Leu 235 (ECL<sub>2</sub>), Leu 236 (ECL<sub>2</sub>), and Gln 234 (ECL<sub>2</sub>) (highlighted with blue circle). The hydrogen bond interactions are indicated by pink dashed lines and the residues involved in hydrogen bonding interactions are displayed in ball and stick format. (B) LigPlot interaction map of PAR2-AABT491 complex. LigPlot map depicting hydrogen bond interactions between AABT 491 and Leu 235 (ECL<sub>2</sub>), Leu 236 (ECL<sub>2</sub>), Gln 234 (ECL<sub>2</sub>) and π-π interaction with Tyr 156<sup>33</sup>, Phe 244<sup>539</sup>. The hydrogen bonding interactions are indicated by pink arrows and π-π interaction in green lines. (For interpretation of the references to color in this figure legend, the reader is referred to the web version of this article.)

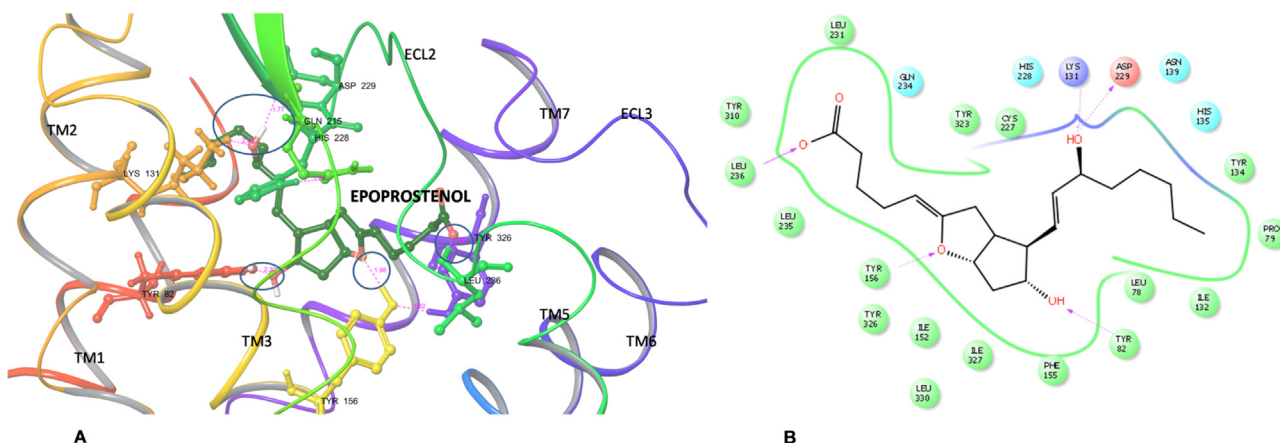


**Fig. 17.** (A) Binding pose of PAR2 model-epoprostenol complex. Binding pose of epoprostenol shows that it forms hydrogen bond with Tyr 82<sup>1,39</sup>, Leu 236 (ECL<sub>2</sub>), Lys131<sup>2,60</sup>, Asp 229 (ECL<sub>2</sub>) and with Tyr 156<sup>3,33</sup> of PAR2 model (highlighted with blue circle). The hydrogen bond interactions are indicated by pink dashed lines and the residues involved in hydrogen bonding interactions are displayed in ball and stick format. (B) LigPlot interaction map of PAR2 model-epoprostenol complex. LigPlot map showing hydrogen bond interaction between epoprostenol and Tyr 82<sup>1,39</sup>, Leu 236 (ECL<sub>2</sub>), Lys131<sup>2,60</sup>, Asp 229 (ECL<sub>2</sub>), Tyr156<sup>3,33</sup> of PAR2 model are depicted by pink arrows. (For interpretation of the references to color in this figure legend, the reader is referred to the web version of this article.)

Binding pose of AABT 491-PAR2 complex shows that AABT 491 was stabilized by hydrogen bonding interactions with Leu 235 (ECL<sub>2</sub>), Leu 236 (ECL<sub>2</sub>) and Gln 234 (ECL<sub>2</sub>). Additionally,  $\pi-\pi$  interaction between Tyr 156<sup>3,33</sup> and Phe 244<sup>5,39</sup> was also observed (Fig. 16A and B). The MDS studies of AABT491 interaction with PAR2 reproduced the interaction with Leu 235 (ECL<sub>2</sub>) Leu 236 (ECL<sub>2</sub>) in most of the frames (Movie M7). Interestingly, PAFR has been associated with tumor development, tumor metastasis, and also in malignant transformation in BRCA1-mutant epithelial ovarian cells. PAFR antagonists were also proved to inhibit cell proliferation in vitro and tumor growth in human breast cancer progression of Ehrlich ascites tumor and melanoma B16F10, thus proving that PAFR-dependent pathways are important in tumor growth [115]. Further studies on the action of PAFR antagonist on PAR2 may explain the efficacy in inhibiting PAR2 signaling.

**3.7.1.4. Ligands belonging to purinoceptors.** P2Y12\_Human – 2-methylthio-ADP methylthio-ADP, epoprostenol, adenosine 5'-O-(3-thiotriphosphate), alpha-thioadenosine triphosphate, clopidogrel, ticlopidine.

P2Y14\_Human – uridine diphosphate galactose, uridine diphosphate glucose, UDP-N-acetylglucosamine, uridine diphosphate glucuronic acid.

P2Y receptor belongs to one of three families of extracellular receptors for purine and pyrimidine nucleotides, involved in purinergic signaling [116]. Eight distinct P2Y receptors are currently recognized: P2Y1, 2, 3, 4, 6, 11, 12, 13 and 14. P2Y12\_Human and P2Y14\_Human receptors were clustered with PARs (Table 2). The study of the binding affinity with the agonist of P2Y12 receptors brought out interesting results. Among the agonists studied, epoprostenol, an agonist of P2Y12 type receptor, showed promising

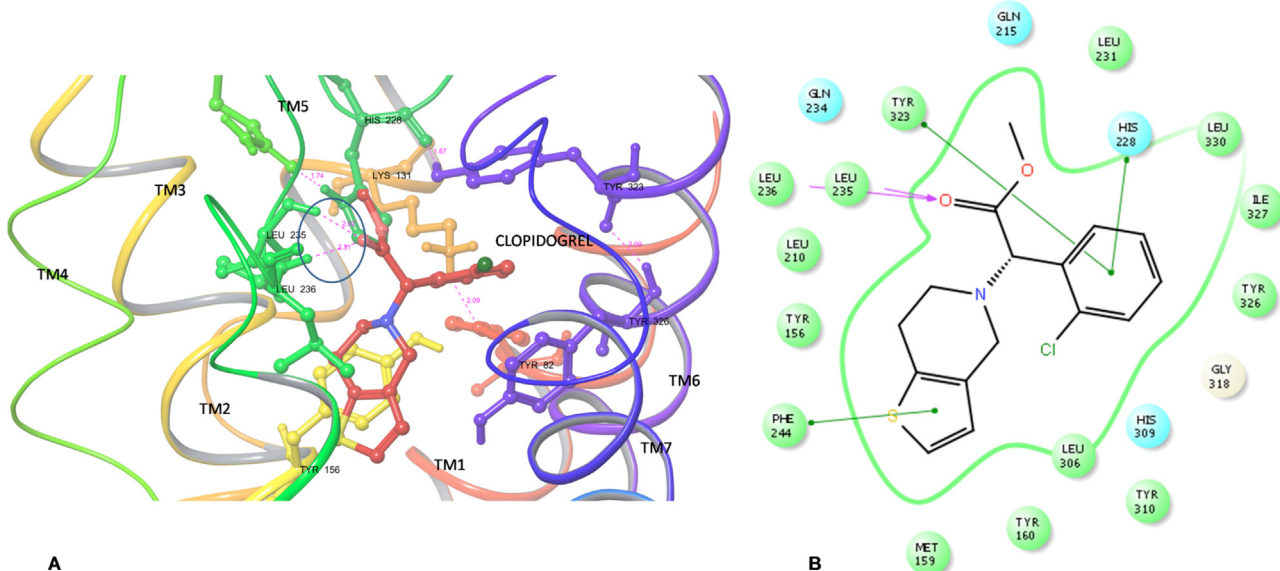


**Fig. 18.** (A) Binding pose of PAR2 model-clopidogrel complex. Binding pose of clopidogrel shows that it forms hydrogen bond with Leu 235 (ECL<sub>2</sub>), and Leu 236 (ECL<sub>2</sub>) of the PAR2 model (highlighted with blue circle). The hydrogen bond interactions are indicated by pink dashed lines and the residues involved in hydrogen bonding interactions are displayed in ball and stick format. (B) LigPlot interaction map of PAR2 model-clopidogrel complex. LigPlot map showing the hydrogen bond interactions of between clopidogrel-Leu 235 (ECL<sub>2</sub>) and Leu 236 (ECL<sub>2</sub>), of PAR2 model are depicted by pink arrows.  $\pi-\pi$  interactions of His 228 (ECL<sub>2</sub>), Phe 244<sup>5,39</sup> and Tyr 323<sup>7,32</sup> with clopidogrel are depicted by green lines. (For interpretation of the references to color in this figure legend, the reader is referred to the web version of this article.)

binding affinity in comparison to 2-methylthio-ADP methylthio-ADP and adenosine 5'-O-(3-thiotriphosphate) (**Table 3**).

The binding pose of epoprostenol showed that it was stabilized by interactions with Tyr 82<sup>1,39</sup>, Leu 236 (ECL<sub>2</sub>), Lys 131<sup>2,60</sup>, Asp 229 (ECL<sub>2</sub>) and Tyr 156<sup>3,33</sup> (**Fig. 17A**). The interaction between Tyr 156<sup>3,33</sup>–Tyr 326<sup>7,35</sup> observed in the apoprotein was retained after docking, indicating that the binding site was close to extracellular loops. It is important to note that this interaction was predicted in our study as one of the interactions important for stabilizing the structure (refer Section 3.4). Importantly, Leu 236 (ECL<sub>2</sub>) was earlier identified as an important residue for binding of vorapaxar in PAR1 crystal structure [31]. Although there are not many studies on the effect of epoprostenol in breast cancer, Med facts study report (<http://medsfacts.com/study-EPOPROSTENOL%20SODIUM-causing-BREAST%20CANCER.php>) relating epoprostenol with increased risk of breast cancer indicates a mechanism that needs further investigation.

The agonists of the P2Y14 receptor included in this study were uridine diphosphate galactose, UDP-N-acetylglucosamine, uridine diphosphate glucuronic acid, UDP-N-acetylglucosamine, 2-methylthio-ADP, adenosine 5'-O-(3-thiotriphosphate), alpha-thioadenosine triphosphate. Among these agonists, uridine diphosphate galactose showed a higher binding affinity in comparison to other agonists (**Table 3**). Molecular dynamics simulation studies showed stable interaction of uridine diphosphate galactose with Gln 317 (ECL<sub>3</sub>) and Lys 315 (ECL<sub>3</sub>) residues of PAR2 (Movie M5). Further studies are required to correlate the high free energy of binding even after stable interaction with residues of ECL<sub>3</sub>.

Ticlopidine and clopidogrel belong to the family of the thienopyridines and are well known antagonist of the P2Y12 receptor. The binding affinity of these antagonists showed promising binding affinity with clopidogrel in comparison to ticlopidine (**Table 3**).

Binding pose of clopidogrel with PAR2 showed that it was stabilized by hydrogen bonding interaction with Leu 235 (ECL<sub>2</sub>) and Leu 236 (ECL<sub>2</sub>) along with π–π interactions between Phe 244<sup>5,39</sup>, His 228 (ECL<sub>2</sub>) and Tyr 323<sup>7,32</sup> (**Fig. 18A and B**). Interestingly, the hydrogen bonding interaction between Tyr 156<sup>3,33</sup> and Tyr 326<sup>7,35</sup> was disrupted possibly due to movement of TMs (the distance between these residues increased to 5.02 Å from 1.809 Å). MDS studies showed stable interaction with Leu 235 (ECL<sub>2</sub>). The stability of the interaction was also confirmed by MDS for 5 ns (Movie M8). In an interesting study, it was observed that the use of ticlopidine and clopidogrel significantly reduced breast cancer-related mortality in women [117]. We suggest that clopidogrel and ticlopidine may act as antagonists to PAR2. However, further experimental studies are necessary to prove the antagonistic activity of ticlopidine/clopidogrel on PAR2.

### 3.7.2. Molecular dynamics studies on PAR2-agonist/antagonist complex

MDS studies with solvating water molecules is a useful method to check the stability of ligand–protein complex as molecular docking usually depicts one of the snapshots of the possible binding modes. MDS studies are acknowledged to be closer to the physiological, environmental conditions, thus revealing near native binding conformations for the docked complex. In this work, MDS study of PAR2 complexed with different ligands was performed to understand the stability of interaction for 5 ns. We limited the simulation time to 5 ns, as this time period was enough to get valuable insights into the receptor–ligand interaction of GPCRs [73,106]. The root mean square deviation (RMSD) on heavy atoms was analyzed, which compares the spatial deviation of structures with respect to time and original structure. The variation of RMSD on heavy atoms in the PAR2-agonists complex (GB110, oleic acid, leukotriene D4, UDP galactose CP5550) and PAR2-antagonists complex (montelukast, AABT 469, clopidogrel) is depicted in Figs. S4 and S5. The

RMSD variations were stabilized at <1.8 Å for oleic acid, CP55950, GB110, UDP galactose, but for leukotriene D4 the complex attained stability slightly above 2 Å (supplementary material, Fig. S4). The final RMSD variation from initial model of heavy atoms of PAR2 model–clopidogrel complex and PAR2 model–montelukast complex was <1.7 Å, and for the PAR2 model–AABT491 complex it was below 2.5 Å (supplementary material, Fig. S5). The MD simulation reproduced most of the docking interaction observed in PAR2 model–agonists complex (GB110, oleic acid, leukotriene D4, UDP galactose, CP5550) (Movies M1–M5) and antagonists (montelukast, AABT 469, clopidogrel) (Movies M6–M8) (discussed in Section 3.7). The root mean square variations were studied on heavy atoms, which gives an idea on how the structures were different from each other. The RMSD on heavy atoms did not change more than 2.5 Å within 5 ns of MD simulation time suggesting the stability of receptor–ligand complex.

This is the first report on the ligands that may show cross reactivity with PAR2, but there are numerous examples among GPCRs. GPR17 was shown to act as common target for the endogenous ligands of nucleotide, cysteinyl-leukotriene and GPR99 receptor [118–120]. Interestingly, P2Y12 receptors respond to a wide array of ligands, which include endogenous ligands of GPCRs of the other families; P2Y12 receptors not only respond to ADP, but also to thrombin, immune complexes, adrenaline, serotonin [121], Thromboxane-A2 and PAR1-selective peptide agonist SFLLRN [122]. Virtual screening methodology and phylogenetic methods led to the identification of cysteinyl leukotrienes and 5-phosphoribosyl 1-pyrophosphate (PRPP) as possible endogenous ligands for P2Y12 [123] and were later proved by experimental studies, showcasing the utility of combining phylogenetic methods and docking method in the identification of ligands (endogenous/synthetic). If one receptor binding to multiple ligands is one side of the complexity, the other side is a single ligand activating additional receptors. Synthetic cannabinoids and leukotrienes were predicted to act by binding to additional receptors [110,118]. Thus, we suggest that PAR2 may respond to ligands of other GPCRs and may show differential signaling or PAR2 may act as additional molecular target for various ligands, to enhance the response in pathophysiological conditions like breast cancer.

## 4. Conclusions

In this work, homology modeling, flexible docking using IFD, calculation of free ligand binding energy and molecular dynamics simulation studies of apoprotein and receptor–ligand complex were undertaken to understand the structure and molecular mechanism of signaling by PAR2.

This study reports an interesting correlation of binding affinity of PAR2 and some of the endogenous ligands (oleic acid, linoleic acid, leukotriene D4, epoprostenol) with already known effects on breast cancer. We propose that these endogenous ligands may bind to PAR2 under some pathological conditions and stabilize the conformational state leading to specific signaling pathways resulting in breast cancer. Interestingly, the promising binding affinity of some of the antagonists studied (montelukast, clopidogrel, AABT 491) with PAR2 also suggests the possible beneficial effects of these drugs in breast cancer therapy. Going beyond, the information in this paper could open up new therapeutic modalities for breast cancer treatment targeting PAR2.

## Acknowledgements

This work is supported by the Department of Science and Technology (SERC), Government of India, Women Scientist Program (WOS-A) Ref. No.: SR/WOS-A/LS-408/2011.

## Appendix A. Supplementary data

Supplementary data associated with this article can be found, in the online version, at <http://dx.doi.org/10.1016/j.jmgm.2014.07.012>.

## References

- [1] F. Gieseler, H. Ungefroren, U. Settmacher, M.D. Hollenberg, R. Kaufmann, Proteinase-activated receptors (PARs) – focus on receptor–receptor-interactions and their physiological and pathophysiological impact, *Cell Commun. Signal.* 11 (2013) 86, <http://dx.doi.org/10.1186/1478-811X-11-86>.
- [2] R. Matej, P. Mandakova, I. Netikova, P. Pouckova, T. Olejar, Proteinase-activated receptor-2 expression in breast cancer and the role of trypsin on growth and metabolism of breast cancer cell line MDA MB-231, *Physiol. Res.* 56 (2007) 475–484.
- [3] M.R. D'Andrea, C.K. Derian, R.J. Santulli, P. Andrade-Gordon, Differential expression of protease-activated receptors-1 and -2 in stromal fibroblasts of normal, benign, and malignant human tissues, *Am. J. Pathol.* 158 (2001) 2031–2041.
- [4] Y. Liu, B.M. Mueller, Protease-activated receptor-2 regulates vascular endothelial growth factor expression in MDA-MB-231 cells via MAPK pathways, *Biochem. Biophys. Res. Commun.* 344 (2006) 1263–1270.
- [5] D. Darmoul, J.C. Marie, H. Devaud, V. Gratio, M. Laburthe, Initiation of human colon cancer cell proliferation by trypsin acting at protease-activated receptor-2, *Br. J. Cancer* 85 (2001) 772–779.
- [6] D.R. Morris, Y. Ding, T.K. Ricks, A. Gullapalli, B.L. Wolfe, J. Trejo, Protease activated receptor-2 is essential for factor VIIa and Xa-induced signaling, migration, and invasion of breast cancer cells, *Cancer Res.* 66 (2006) 307–314.
- [7] D. Darmoul, V. Gratio, H. Devaud, M. Laburthe, Protease-activated receptor 2 in colon cancer–trypsin induced MAPK phosphorylation and cell proliferation are mediated by epidermal growth factor receptor transactivation, *J. Biol. Chem.* 279 (2006) 20927–20934.
- [8] S. Miyata, N. Koshikawa, H. Yasumitsu, K. Miyazaki, Trypsin stimulates integrin α5β1-dependent adhesion to fibronectin and proliferation of human gastric carcinoma cells through activation of proteinase-activated receptor-2, *J. Biol. Chem.* 275 (2000) 4592–4598.
- [9] R. Shimamoto, T. Sawada, Y. Uchima, M. Inoue, K. Kimura, Y. Yamashita, N. Yamada, T. Nishihara, M. Ohira, K. Hirakawa, A role for protease-activated receptor-2 in pancreatic cancer cell proliferation, *Int. J. Oncol.* 24 (2004) 1401–1406.
- [10] T. Ohta, K. Shimizu, S. Yi, H. Takamura, K. Amaya, H. Kitagawa, M. Kayahara, I. Ninomiya, S. Fushida, T. Fujimura, G. Nishimura, K. Miwa, Protease-activated receptor-2 expression and the role of trypsin in cell proliferation in human pancreatic cancers, *Int. J. Oncol.* 23 (2003) 61–66.
- [11] G. Jin, T. Hayashi, J. Kawagoe, T. Takizawa, T. Nagata, I. Nagano, M. Syoji, K. Abe, Deficiency of PAR2 gene increases acute focal ischemic brain injury, *J. Cereb. Blood Flow Metab.* 25 (2005) 302–313.
- [12] S. Su, Y. Li, Y. Luo, Y. Sheng, Y. Su, R.N. Padia, Z.K. Pan, Z. Dong, S. Huang, Proteinase-activated receptor 2 expression in breast cancer and its role in breast cancer cell migration, *Oncogene* 28 (2009) 3047–3057.
- [13] G.M. Hjortoe, L.C. Petersen, T. Albrektsen, B.B. Sorensen, P.L. Norby, S.K. Mandal, U.R. Pendurthi, L.V. Rao, Tissue factor-factor VIIa-specific up-regulation of IL-8 expression in MDA-MB-231 cells is mediated by PAR-2 and results in increased cell migration, *Blood* 103 (2004) 3029–3037.
- [14] L. Ge, Y. Ly, M. Hollenberg, K. Defea, A beta-arrestin-dependent scaffold is associated with prolonged MAPK activation in pseudopodia during protease activated receptor-2-induced chemotaxis, *J. Biol. Chem.* 278 (2003) 34418–34426.
- [15] N. Parisi, G. Metodieva, M.V. Metodiev, Pseudopodial and β-arrestin-interacting proteomes from migrating breast cancer cells upon PAR2 activation, *J. Proteomics* 80C (2013) 91–106.
- [16] S. Nystedt, K. Emilsson, A.K. Larsson, B. Strömbeck, J. Sundelin, Molecular cloning and functional expression of the gene encoding the human proteinase-activated receptor 2, *Eur. J. Biochem.* 232 (1995) 84–89.
- [17] S.R. Coughlin, Thrombin signalling and protease-activated receptors, *Nature* 407 (2000) 258–264.
- [18] M. Molino, E.S. Barnathan, R. Numerof, J. Clark, M. Dreyer, A. Cumashi, J.A. Hoxie, N. Schechter, M. Woolkalis, L.F. Brass, Interactions of mast cell tryptase with thrombin receptors and PAR-2, *J. Biol. Chem.* 272 (1997) 4043–4049.
- [19] E. Camerer, W. Huang, S.R. Coughlin, Tissue factor- and factor X-dependent activation of protease-activated receptor 2 by factor VIIa, *Proc. Natl. Acad. Sci. U.S.A.* 97 (2000) 5255–5260.
- [20] R. Smith, A. Jenkins, A. Lourbakos, P. Thompson, V. Ramakrishnan, J. Tomlinson, U. Deshpande, D.A. Johnson, R. Jones, E.J. Mackie, R.N. Pike, Evidence for the activation of PAR-2 by the sperm protease, acrosin: expression of the receptor on oocytes, *FEBS Lett.* 484 (2000) 285–290.
- [21] T. Takeuchi, J.L. Harris, W. Huang, K.W. Yan, S.R. Coughlin, C.S. Craik, Cellular localization of membrane-type serine protease and identification of protease activated receptor-2 and single chain urokinase-type plasminogen activator as substrates, *J. Biol. Chem.* 275 (2000) 26333–26342.
- [22] K.K. Hansen, P.M. Sherman, L. Cellars, P. Andrade-Gordon, Z. Pan, A. Baruch, J.L. Wallace, M.D. Hollenberg, N. Vergnolle, A major role for proteolytic activity and proteinase-activated receptor-2 in the pathogenesis of infectious colitis, *Proc. Natl. Acad. Sci. U.S.A.* 102 (2005) 8363–8368.
- [23] G.J. Mize, W. Wang, T.K. Takayama, Prostate-specific kallikreins-2 and -4 enhance the proliferation of DU-145 prostate cancer cells through protease-activated receptors-1 and 2, *Mol. Cancer Res.* 6 (2008) 1043–1051.
- [24] A.J. Ramsay, Y. Dong, M.L. Hunt, M. Linn, H. Samaratunga, J.A. Clements, J.D. Hooper, Kallikrein-related peptidase 4 (KLK4) initiates intracellular signaling via protease-activated receptors (PARs). KLK4 and PAR-2 are co-expressed during prostate cancer progression, *J. Biol. Chem.* 283 (2008) 12293–12304.
- [25] K. Oikonomopoulou, K.K. Hansen, M. Saifeddine, I. Tea, M. Blaber, S.I. Blaber, I. Scarisbrick, P. Andrade-Gordon, G.S. Cottrell, N.W. Bunnett, E.P. Diamandis, M.D. Hollenberg, Proteinase-activated receptors, targets for kallikrein signaling, *J. Biol. Chem.* 281 (2006) 32095–32112.
- [26] S.P. Alexander, A. Mathie, J.A. Peters, Guide to receptors and channels (GRAC) 3rd edition, *Br. J. Pharmacol.* 153 (Suppl. 2) (2008) S1–S209.
- [27] T.K. Vu, D.T. Hung, V.I. Wheaton, S.R. Coughlin, Molecular cloning of a functional thrombin receptor reveals a novel proteolytic mechanism of receptor activation, *Cell* 64 (1991) 1057–1068.
- [28] T.K. Vu, V.I. Wheaton, D.T. Hung, I. Charo, S.R. Coughlin, Domains specifying thrombin-receptor interaction, *Nature* 353 (1991) 674–677.
- [29] S.R. Macfarlane, J. Michael, M.J. Seatter, T. Kanke, G.D. Hunter, R. Plevin, Proteinase-activated receptors, *Pharmacol. Rev.* 53 (2001) 245–282.
- [30] M.N. Adams, R. Ramachandran, M.K. Yau, J.Y. Suen, D.P. Fairlie, M.D. Hollenberg, J.D. Hooper, Structure, function and pathophysiology of protease activated receptors, *Pharmacol. Ther.* 130 (2011) 248–282.
- [31] C. Zhang, Y. Srinivasan, D.H. Arlow, J.J. Fung, D. Palmer, Y. Zheng, H.F. Green, A. Pandey, R.O. Dror, D.E. Shaw, W.I. Weis, S.R. Coughlin, B.K. Kobilka, High-resolution crystal structure of human protease-activated receptor, *Nature* 492 (2012) 387–392.
- [32] R. Ramachandran, M.D. Hollenberg, Proteinases and signalling: pathophysiological and therapeutic implications via PARs and more, *Br. J. Pharmacol.* 153 (2008) S263–S282.
- [33] L.M. Sevigny, P. Zhang, A. Bohm, K. Lazarides, G. Perides, L. Covic, A. Kulipolous, Interdicting protease-activated receptor-2-driven inflammation with cell-penetrating pepducins, *Proc. Natl. Acad. Sci. U.S.A.* 108 (2011) 8491–8496.
- [34] J.Y. Suen, G.D. Barry, R.J. Lohman, M.A. Halili, A.J. Cotterell, G.T. Le, D.P. Fairlie, Modulating human proteinase activated receptor 2 with a novel antagonist (GB88) and agonist (GB110), *Br. J. Pharmacol.* 165 (2012) 1413–1423, <http://dx.doi.org/10.1111/j.1476-5381.2011.01610.x>.
- [35] G.D. Barry, J.Y. Suen, G.T. Le, A. Cotterell, R.C. Reid, D.P. Fairlie, Novel agonists and antagonists for human protease activated receptor 2, *J. Med. Chem.* 53 (2010) 7428–7440.
- [36] M.P. Jacobson, R.A. Friesner, Z. Xiang, B. Honig, On the role of crystal packing forces in determining protein side chain conformations, *J. Mol. Biol.* 320 (2002) 597–608.
- [37] M.P. Jacobson, D.L. Pincus, C.S. Rapp, T.J.F. Day, B. Honig, D.E. Shaw, R.A. Friesner, A hierarchical approach to all-atom protein loop prediction, *Proteins* 55 (2004) 351–367.
- [38] J.D. Thompson, D.G. Higgins, T.J. Gibson, CLUSTAL W: improving the sensitivity of progressive multiple sequence alignment through sequence weighting, position-specific gap penalties and weight matrix choice, *Nucleic Acids Res.* 22 (1994) 4673–4680.
- [39] J.L. Banks, H.S. Beard, Y. Cao, A.E. Cho, Damm, R. Farid, A.K. Felts, T.A. Halgren, D.T. Mainz, J.R. Maple, R. Murphy, D.M. Philipp, M.P. Repasky, L.Y. Zhang, B.J. Berne, R.A. Friesner, E. Gallicchio, R.M. Levy, Integrated modeling program, applied chemical theory (IMPACT), *J. Comput. Chem.* 26 (2005) 1752–1780.
- [40] R.A. Laskowski, M.W. MacArthur, D.S. Moss, J.M. Thornton, PROCHECK: a program to check the stereochemical quality of protein structures, *J. Appl. Cryst.* 26 (1993) 283–291.
- [41] M.J. Sippl, Recognition of errors in three-dimensional structures of proteins, *Proteins* 17 (1993) 355–362.
- [42] M. Wiederstein, M.J. Sippl, ProSA-web: interactive web service for the recognition of errors in three-dimensional structures of proteins, *Nucleic Acids Res.* 35 (2007) W407–W410.
- [43] C. Colovos, T.O. Yeates, Verification of protein structures: patterns of non-bonded atomic interaction, *Protein Sci.* 2 (1993) 1511–1519.
- [44] V.B. Chen, W.B. Arendall 3rd, J.J. Headd, D.A. Keedy, R.M. Immormino, G.J. Kapral, L.W. Murray, J.S. Richardson, D.C. Richardson, MolProbity: all-atom structure validation for macromolecular crystallography, *Acta Crystallogr. D: Biol. Crystallogr.* 66 (2010) 12–21.
- [45] D. Shivakumar, J. Williams, Y. Wu, W. Damm, J. Shelley, W. Sherman, Prediction of absolute solvation free energies using molecular dynamics free energy perturbation and the OPLS force field, *J. Comput. Aided Mol. Des.* 6 (2010) 1509–1519.
- [46] Z. Guo, U. Mohanty, J. Noehre, T.K. Sawyer, W. Sherman, G. Krilov, Probing the α-helical structural stability of stapled p53 peptides: molecular dynamics simulations and analysis, *Chem. Biol. Drug Des.* 75 (2010) 348–359.
- [47] J.B. Kevin, C. Edmond, X. Huafeng, O.D. Ron, P.E. Michael, A.G. Brent, L.K. John, K. Istvan, A.M. Mark, D.S. Federico, K.S. John, S. Yibing, E.S. David, Scalable algorithms for molecular dynamics simulations on commodity clusters, in: *Proceedings of the 2006 ACM/IEEE Conference on Supercomputing, Tampa, ACM, Florida, 2006*.
- [48] W.G. Hoover, Canonical dynamics: equilibrium phase-space distributions, *Phys. Rev. A (American Physical Society)* 31 (1985) 1695–1697.

- [49] K.K. Kakarala, K. Jamil, Sequence-structure based phylogeny of GPCR Class A Rhodopsin receptors, *Mol. Phylogenet. Evol.* 74 (2014) 66–96.
- [50] Y. Okuno, A. Tamon, H. Yabuuchi, S. Niijima, Y. Minowa, K. Tonomura, R. Kunimoto, C. Feng, GLIDA: GPCR – ligand database for chemical genomics drug discovery – database and tools update, *Nucleic Acids Res.* 36 (2008) D907–D912.
- [51] P.D. Lyne, M.L. Lamb, J.C. Saeh, Accurate prediction of the relative potencies of members of a series of kinase inhibitors using molecular docking and MM-GBSA scoring, *J. Med. Chem.* 49 (2006) 4805–4808.
- [52] J.A. Ballesteros, H. Weinstein, C.S. Stuart, Integrated methods for the construction of three-dimensional models and computational probing of structure–function relations in G protein coupled receptors, *Methods Neurosci.* 25 (1995) 366–428.
- [53] A.S. Rothmeier, W. Ruf, Protease-activated receptor 2 signaling in inflammation, *Semin. Immunopathol.* 34 (2012) 133–149.
- [54] J.Y. Suen, B. Gardiner, S. Grimmond, D.P. Fairlie, Profiling gene expression induced by protease-activated receptor 2 (PAR2) activation in human kidney cells, *PLoS ONE* 5 (2010) e13809.
- [55] S. Costanzi, On the applicability of GPCR homology models to computer-aided drug discovery: a comparison between *in silico* and crystal structures of the beta2-adrenergic receptor, *J. Med. Chem.* 51 (2008) 2907–2914.
- [56] M. Michino, E. Abola, GPCR Dock 2008 participants, C.L. Brooks 3rd, J.S. Dixon, J. Moult, R.C. Stevens, Community-wide assessment of GPCR structure modelling and ligand docking: GPCR Dock 2008, *Nat. Rev. Drug Discov.* 8 (2009) 455–463.
- [57] J. Carlsson, R.G. Coleman, V. Setola, J.J. Irwin, H. Fan, A. Schlessinger, A. Sali, B.L. Roth, B.K. Shoichet, Ligand discovery from a dopamine D3 receptor homology model and crystal structure, *Nat. Chem. Biol.* 7 (2011) 769–778.
- [58] A.J. Kooistra, L. Roumen, R. Leurs, I.J. de Esch, C. de Graaf, From heptahelical bundle to hits from the Haystack: structure-based virtual screening for GPCR ligands, *Methods. Enzymol.* 522 (2013) 279–336, <http://dx.doi.org/10.1016/B978-0-12-407865-9.00015-7>.
- [59] M.K. Yau, L. Liu, D.P. Fairlie, Toward drugs for protease-activated receptor 2 (PAR2), *J. Med. Chem.* 56 (2013) 7477–7497, <http://dx.doi.org/10.1021/jm400638v> (Epub 2013 July 30).
- [60] T. Beuming, W. Sherman, Current assessment of docking into GPCR crystal structures and homology models: successes, challenges, and guidelines, *J. Chem. Inf. Model.* 52 (2012) 3263–3277.
- [61] J.C. Mobarec, R. Sanchez, M. Filizola, Modern homology modeling of G-protein coupled receptors: which structural template to use? *J. Med. Chem.* 52 (2009) 5207–5216.
- [62] B. Wu, E.Y. Chien, C.D. Mol, G. Fenalti, W. Liu, V. Katritch, R. Abagyan, A. Brooun, P. Wells, F.C. Bi, D.J. Hamel, P. Kuhn, T.M. Handel, V. Cherezov, R.C. Stevens, Structures of the CXCR4 chemokine GPCR with small-molecule and cyclic peptide antagonists, *Science* 330 (November (6007)) (2010) 1066–1071, <http://dx.doi.org/10.1126/science.1194396> (Epub 2010 October 7).
- [63] A. Manglik, A.C. Kruse, T.S. Kobilka, F.S. Thian, J.M. Mathiesen, R.K. Sunahara, L. Pardo, W.I. Weis, B.K. Kobilka, S. Granier, Crystal structure of the micro-opioid receptor bound to a morphinan antagonist, *Nature* 485 (2012) 321–326.
- [64] H. Wu, D. Wacker, M. Mileni, V. Katritch, G.W. Han, E. Vardy, W. Liu, A.A. Thompson, X.P. Huang, F.I. Carroll, S.W. Mascarella, R.B. Westkaemper, P.D. Moser, B.L. Roth, V. Cherezov, R.C. Stevens, Structure of the human κ-opioid receptor in complex with JDTic, *Nature* 485 (2012) 327–332.
- [65] M.C. Peeters, G.J. Pvan Westen, Q. Li, A.P. Ijzerman, Importance of the extracellular loops in G protein-coupled receptors for ligand recognition and receptor activation, *Trends Pharmacol. Sci.* 32 (2011) 35–42.
- [66] K. Zhu, D.L. Pincus, S. Zhao, S.R.A. Friesner, Long loop prediction using the protein local optimization program, *Proteins: Struct. Funct. Bioinform.* 65 (2006) 438–452.
- [67] D.A. Goldfeld, K. Zhu, T. Beuming, R.A. Friesner, Successful prediction of the intra- and extracellular loops of four G-protein coupled receptors, *Proc. Natl. Acad. Sci. U.S.A.* 108 (2011) 8275–8280.
- [68] D. Pal, P. Chakrabarti, On residues in the disallowed region of the Ramachandran map, *Biopolymers* 63 (2002) 195–206.
- [69] T. Yarnitzky, A. Levi, M.Y. Niv, Homology modeling of G-protein-coupled receptors with X-ray structures on the rise, *Curr. Opin. Drug Discov. Devel.* 13 (2010) 317–325.
- [70] J.M. Johnston, M. Filizola, Showcasing modern molecular dynamics simulations of membrane proteins through G protein-coupled receptors, *Curr. Opin. Struct. Biol.* 21 (2011) 552–558.
- [71] E. Jo, B. Bhattacharai, E. Repetto, M. Guerrero, S. Riley, S.J. Brown, Y. Kohno, E. Roberts, S.C. Schürer, H. Rosen, Novel selective allosteric and bitopic ligands for the S1P(3) receptor, *ACS Chem. Biol.* 7 (2012) 1975–1983.
- [72] A. Raval, S. Piana, M.P. Eastwood, R.O. Dror, D.E. Shaw, Refinement of protein structure homology models via long, all-atom molecular dynamics simulations, *Proteins* 80 (2012) 2071–2079.
- [73] C.B. Platania, S. Salomone, G.M. Leggio, F. Drago, C. Bucolo, Homology modeling of dopamine D2 and D3 receptors: molecular dynamics refinement and docking evaluation, *PLoS One* 7 (2012) e44316, <http://dx.doi.org/10.1371/journal.pone.0044316> (Epub 2012 September 6. Erratum in: *PLoS One* 8(1) 2013).
- [74] S. Radestock, T. Weil, S. Renner, Homology model-based virtual screening for GPCR ligands using docking and target-biased scoring, *J. Chem. Inf. Model.* 48 (2008) 1104–1117.
- [75] V. Katritch, M. Rueda, P.C. Lam, M. Yeager, R. Abagyan, GPCR 3D homology models for ligand screening: lessons learned from blind predictions of adenosine A2A receptor complex, *Protein* 78 (2010) 197–211.
- [76] C.N. Cavasotto, A.J. Orry, N.J. Murgolo, Discovery of novel chemotypes to a G-protein-coupled receptor through ligand-steered homology modeling and structure-based virtual screening, *J. Med. Chem.* 51 (2008) 581–588.
- [77] S.S. Phatak, E.A. Gatica, C.N. Cavasotto, Ligand-steered modeling and docking: a benchmarking study in Class A G-protein-coupled receptors, *J. Chem. Inf. Model.* 50 (2010) 2119–2128.
- [78] P. Diaz, S.S. Phatak, J. Xu, F. Astruc-Diaz, C.N. Cavasotto, M. Naguib, 6-Methoxy-N-alkyl isatin acylhydrazone derivatives as a novel series of potent selective cannabinoid receptor 2 inverse agonists: design, synthesis and binding mode prediction, *J. Med. Chem.* 52 (2009) 433–444.
- [79] P. Diaz, S.S. Phatak, J. Xu, et al., 2,3-Dihydro-1-benzofuran derivatives as a series of potent selective cannabinoid receptor 2 agonists: design, synthesis, and binding mode prediction through ligand-steered modeling, *Chem. Med. Chem.* 4 (2009) 1615–1629.
- [80] S. Lorenzen, Y. Zhang, Identification of near-native structures by clustering protein docking conformations, *Proteins* 68 (2007) 187–194.
- [81] R.A. Friesner, J.L. Banks, R.B. Murphy, T.A. Halgren, J.J. Klicic, D.T. Mainz, M.P. Repasky, E.H. Knoll, M. Shelley, J.K. Perry, D.E. Shaw, P. Francis, P.S. Shenkin, Glide: a new approach for rapid, accurate docking and scoring. Method and assessment of docking accuracy, *J. Med. Chem.* 47 (2004) 1739–1749.
- [82] R.A. Friesner, R.B. Murphy, M.P. Repasky, L.L. Frye, J.R. Greenwood, T.A. Halgren, P.C. Sanschagrin, D.T. Mainz, Extra precision glide: docking and scoring incorporating a model of hydrophobic enclosure for protein-ligand complexes, *J. Med. Chem.* 49 (2006) 6177–6196.
- [83] P. Plenge, L. Shi, T. Beuming, J. Te, A.H. Newman, H. Weinstein, U. Gether, C.J. Loland, Steric hindrance mutagenesis in the conserved extracellular vestibule impedes allosteric binding of antidepressants to the serotonin transporter, *J. Biol. Chem.* 287 (2012) 39316–39326.
- [84] D. Pala, T. Beuming, W. Sherman, A. Lodola, S. Rivara, M. Mor, Structure-based virtual screening of MT2 melatonin receptor: influence of template choice and structural refinement, *J. Chem. Inf. Model.* 53 (2013) 821–835.
- [85] R. Farid, T. Day, R.A. Friesner, R.A. Pearlstein, New insights about HERG blockade obtained from protein modeling, potential energy mapping, and docking studies, *Bioorg. Med. Chem.* 14 (2006) 3160–3173.
- [86] F.M. McRobb, B. Capuano, I.T. Crosby, D.K. Chalmers, E. Yuriev, Homology, Modeling and docking evaluation of aminergic G protein-coupled receptors, *J. Chem. Inf. Model.* 50 (2010) 626–637.
- [87] J. Yoo, J.L. Medina-Franco, Homology modeling, docking and structure-based pharmacophore of inhibitors of DNA methyltransferase, *J. Comput. Aided Mol. Des.* 25 (2010) 555–567.
- [88] G. Rastelli, R.A. Del, G. Degliesposti, M.S. Gobba, Fast and accurate predictions of binding free energies using MM-PBSA and MM-GBSA, *J. Comput. Chem.* 31 (2010) 797–810.
- [89] B. Balaji, M. Ramanathan, Prediction of estrogen receptor β ligands potency and selectivity by docking and MM-GBSA scoring methods using three different scaffolds, *J. Enzyme Inhib. Med. Chem.* 27 (2012) 832–844.
- [90] S. Bockenhauer, A. Fürstenberg, X.J. Yao, B.K. Kobilka, W.E. Moerner, Conformational dynamics of single G protein-coupled receptors in solution, *J. Phys. Chem. B* 115 (2011) 13328–13338.
- [91] S. Granier, B. Kobilka, A new era of GPCR structural and chemical biology, *Nat. Chem. Biol.* 8 (2012) 670–673.
- [92] R.U. Malik, M. Ritt, B.T. DeVree, R.R. Neubig, R.K. Sunahara, S. Sivaramakrishnan, Detection of G protein-selective G protein-coupled receptor (GPCR) conformations in live cells, *J. Biol. Chem.* 288 (2013) 17167–17178.
- [93] B. Trzaskowski, D. Latek, S. Yuan, U. Ghoshdastider, A. Debinski, S. Filippek, Action of molecular switches in GPCRs – theoretical and experimental studies, *Curr. Med. Chem.* 19 (2012) 1090–1109.
- [94] X. Deupi, J. Standfuss, Structural insights into agonist-induced activation of G-protein-coupled receptors, *Curr. Opin. Struct. Biol.* 21 (1996) (2011) 541–551.
- [95] Z. Markovic-Housley, B. Stolz, R. Lanz, B. Erni, Effects of tryptophan to phenylalanine substitutions on the structure, stability, and enzyme activity of the IIAB(Man) subunit of the mannose transporter of *Escherichia coli*, *Protein Sci.* 8 (1999) 1530–1535.
- [96] D.L. Farrens, C. Altenbach, K. Yang, W.L. Hubbell, H.G. Khorana, Requirement of rigid-body motion of transmembrane helices for light activation of rhodopsin, *Science* 274 (1996) 768–770.
- [97] T.D. Dunham, D.L. Farrens, Conformational changes in rhodopsin. Movement of helix f detected by site-specific chemical labeling and fluorescence spectroscopy, *J. Biol. Chem.* 274 (1999) 1683–1690.
- [98] J.C. Fowler, S. Bhattacharya, J.D. Urban, N. Vaidehi, R.B. Mailman, Receptor conformations involved in dopamine D(2L) receptor functional selectivity induced by selected transmembrane-5 serine mutations, *Mol. Pharmacol.* 81 (2012) 820–831.
- [99] J. Emmerich, G. Chadeuf, M.J. Coetze, M. Alhenc-Gelas, J.N. Fiessinger, M. Aiach, A phenylalanine 402 to leucine mutation is responsible for a stable inactive conformation of antithrombin, *Thromb. Res.* 76 (1994) 307–315.
- [100] P. Joost, A. Methner, Phylogenetic analysis of 277 human G-protein-coupled receptors as a tool for the prediction of orphan receptor ligands, *Genome Biol.* 3 (2002), Research0063–Research0063.16.
- [101] R. Metpally, R. Sowdhamini, Cross genome phylogenetic analysis of human and *Drosophila* G protein-coupled receptors: application to functional annotation of orphan receptors, *BMC Genom.* 6 (2005) 1–20.

- [102] E. van der Horst, J.E. Peironcely, A.P. Ijzerman, M.W. Beukers, J.R. Lane, H.W. van Vlijmen, M.T. Emmerich, Y. Okuno, A. Bender, A novel chemogenomics analysis of G protein-coupled receptors (GPCRs) and their ligands: a potential strategy for receptor de-orphanization, *BMC Bioinform.* 11 (2010) 316.
- [103] O. Civelli, R.K. Reinscheid, Y. Zhang, Z. Wang, R. Fredriksson, H.B. Schiöth, G protein-coupled receptor deorphanizations, *Annu. Rev. Pharmacol. Toxicol.* 53 (2013) 127–146.
- [104] S. Hardy, G.G. St-Onge, E. Joly, Y. Langelier, M. Prentki, Oleate promotes the proliferation of breast cancer cells via the G protein-coupled receptor GPR40, *J. Biol. Chem.* 280 (2005) 13285–13291.
- [105] D.P. Rose, J.M. Connolly, X.H. Liu, Effects of linoleic acid on the growth and metastasis of two human breast cancer cell lines in nude mice and the invasive capacity of these cell lines in vitro, *Cancer Res.* 54 (1994) 6557–6562.
- [106] C. Parravicini, G. Ranghino, M.P. Abbracchio, P. Fantucci, GPR17: molecular modeling and dynamics studies of the 3-D structure and purinergic ligand binding features in comparison with P2Y receptors, *BMC Bioinform.* 263 (2008), <http://dx.doi.org/10.1186/1471-2105-9-263>.
- [107] R.K. Singh, S. Gupta, S. Dastidar, A. Ray, Cysteinyl leukotrienes and their receptors: molecular and functional characteristics, *Pharmacology* 85 (2010) 336–349.
- [108] M. Bäck, T. Shimizu, T. Yokomizo, G.E. Rovati, C.N. Serhan, S.-E. Dahlén, J. Drazen, J.F. Evans, W. Powell, Leukotriene receptors, introduction, 2013. Last modified on 08/10/2013. <http://www.iuphar-db.org/DATABASE/FamilyIntroductionForward?familyId=35>
- [109] J.R. Lindner, M.L. Kahn, S.R. Coughlin, G.R. Sambrano, E. Schauble, D. Bernstein, D. Foy, A. Hafezi-Moghadam, K. Ley, Delayed onset of inflammation in protease-activated receptor-2-deficient mice, *J. Immunol.* 165 (2001) 6504–6510.
- [110] C. Magnusson, J. Liu, R. Ehrnström, J. Manjer, K. Jirström, T. Andersson, A. Sjölander, Cysteinyl leukotriene receptor expression pattern affects migration of breast cancer cells and survival of breast cancer patients, *Int. J. Cancer* 129 (2011) 9–22.
- [111] Z. Qamri, A. Preet, M.W. Nasser, C.E. Bass, G. Leone, S.H. Barsky, R.K. Ganju, Synthetic cannabinoid receptor agonists inhibit tumor growth and metastasis of breast cancer, *Mol. Cancer Ther.* 8 (2009) 3117–3129.
- [112] M.M. Caffarel, C. Andradas, E. Pérez-Gómez, M. Guzmán, C. Sánchez, Cannabinoids: a new hope for breast cancer therapy? *Cancer Treat. Rev.* 38 (2012) 911–918.
- [113] R.G. Pertwee, A.C. Howlett, M.E. Abood, S.P. Alexander, V. Di Marzo, M.R. Elphick, P.J. Greasley, H.S. Hansen, G. Kunos, K. Mackie, R. Mechoulam, R.A. Ross, International Union of Basic and Clinical Pharmacology, LXXIX. Cannabinoid receptors and their ligands: beyond CB<sub>1</sub> and CB<sub>2</sub>, *Pharmacol. Rev.* 62 (2010) 588–631.
- [114] E. Ninio, S. Jancar, F.J.O. Rios, T. McIntyre, C. O'Neill, J.B. Travers, Platelet-activating factor receptor, introduction. Last modified on 03/06/2013. <http://www.iuphar-db.org/DATABASE/FamilyIntroductionForward?familyId=55>
- [115] C. Cellai, A. Laurenzana, A.M. Vannucchi, R. Caporale, M. Paglierani, S. Di Lollo, A. Pancrazi, F. Paoletti, Growth inhibition and differentiation of human breast cancer cells by the PAFR antagonist WEB-2086, *Br. J. Cancer* 94 (2006) 1637–1642.
- [116] G. Burnstock, The past, present and future of purine nucleotides as signalling molecules, *Neuropharmacology* 36 (1997) 1127–1139.
- [117] G.N. Armaiz-Pena, J.K. Allen, A. Cruz, R.L. Stone, A.M. Nick, Y.G. Lin, L.Y. Han, L.S. Mangala, C.J. Villares, P. Vivas-Mejia, C. Rodriguez-Aguayo, A.S. Nagaraja, K.M. Gharpure, Z. Wu, R.D. English, K.V. Soman, M.M. Shahzad, M. Zigler, M.T. Deavers, A. Zien, T.G. Soldatos, D.B. Jackson, J.E. Wiktorowicz, M. Torres-Lugo, T. Young, K. De Geest, G.E. Gallick, M. Bar-Eli, G. Lopez-Berestein, S.W. Cole, G.E. Lopez, S.K. Lutgendorf, A.K. Sood, Src activation by β-adrenoreceptors is a key switch for tumour metastasis, *Nat. Commun.* 49 (2013) 1403.
- [118] V. Capra, S. Ravasi, M.R. Accomazzo, S. Citro, M. Grimoldi, M.P. Abbracchio, G.E. Rovati, CysLT1 receptor is a target for extracellular nucleotide-induced heterologous desensitization: a possible feedback mechanism in inflammation, *J. Cell Sci.* 1 (2005) 5625–5636.
- [119] P. Ciana, M. Fumagalli, M.L. Trincavelli, C. Verderio, P. Rosa, D. Lecca, S. Ferrario, C. Parravicini, V. Capra, P. Gelosa, U. Guerrini, S. Belcredito, M. Cimino, L. Sironi, E. Tremoli, G.E. Rovati, C. Martini, M.P. Abbracchio, The orphan receptor GPR17 identified as a new dual uracil nucleotides/cysteinyl-leukotrienes receptor, *EMBO J.* 25 (2006) 4615–4627 (Epab 2006 September 21).
- [120] M. Bäck, T. Shimizu, T. Yokomizo, G.E. Rovati, C.N. Serhan, S.-E. Dahlén, J. Drazen, J.F. Evans, W. Powell, Leukotriene receptors, introduction. Last modified on 08/10/2013. <http://www.iuphar-db.org/DATABASE/FamilyIntroductionForward?familyId=35>
- [121] R.F. Storey, H.M. Judge, R.G. Wilcox, S. Heptinstall, Inhibition of ADP-induced P-selectin expression and platelet-leukocyte conjugate formation by clopidogrel and the P2Y12 receptor antagonist AR-C69931MX but not aspirin, *Thromb. Haemost.* 88 (2002) 488–494.
- [122] S.P. Kunapuli, R.T. Dorsam, S. Kim, T.M. Quinton, Platelet purinergic receptors, *Curr. Opin. Pharmacol.* 3 (2003) 175–180.
- [123] Y. Nonaka, T. Hiramoto, N. Fujita, Identification of endogenous surrogate ligands for human P2Y12 receptors by *in silico* and *in vitro* methods, *Biochem. Biophys. Res. Commun.* 337 (2005) 281–288.